



IMPLEMENTATION OF AN AUTONOMOUS STAR RECOGNITION ALGORITHM USING HARDWARE-SOFTWARE CO-PROCESSING APPROACH

**DANG LE DANG KHOA
G1500337L**

**SCHOOL OF ELECTRICAL AND ELECTRONICS ENGINEERING
2018**

IMPLEMENTATION OF AN AUTONOMOUS STAR RECOGNITION ALGORITHM USING HARDWARE-SOFTWARE CO-PROCESSING APPROACH

by

DANG LE DANG KHOA

Supervisor: Asst. Prof. Chen Shoushun

Co-Supervisor: Assoc. Prof. Goh Wang Ling

A thesis submitted to the
Nanyang Technological University
in partial fulfilment of the
requirements for the degree of
Master of Engineering

School of Electrical and Electronics Engineering
Nanyang Technological University

2018

Statement of Originality

I hereby certify that the work embodied in this thesis is the result of original research, is free of plagiarised materials, and has not been submitted for a higher degree to any other University or Institution.

.....

Date

.....

Dang Le Dang Khoa

Supervisor Declaration Statement

I have reviewed the content and presentation style of this thesis and declare it is free of plagiarism and of sufficient grammatical clarity to be examined. To the best of my knowledge, the research and writing are those of the candidate except as acknowledged in the Author Attribution Statement. I confirm that the investigations were conducted in accord with the ethics policies and integrity standards of Nanyang Technological University and that the research data are presented honestly and without prejudice.

.....

Date

.....

Assoc Prof Chen Shoushun

Abstract

Implementation of An Autonomous Star Recognition Algorithm using Hardware-Software Co-Processing Approach

By Dang Le Dang Khoa

There are various types of Attitude Determination sensors such as sun sensors, magnetometer, RF beacon but only Star Trackers can achieve the accuracy to arc seconds. A Star Tracker is an embedded system mounted on a spacecraft comprised of an Image sensor and a Computer. It helps determine the attitude of the satellite based on an Autonomous Star Recognition Algorithm. The Star Sensor would take an image of stars at its current position, and then the star pattern recognition algorithms would extract features to construct a pattern from the images. This pattern then is compared with a prebuilt Star Pattern Database (SPD) to return the Star Identity of a star in the Image. This star identity is an important part to determine the attitude of the satellite.

To implement the Algorithm on a specific hardware, the computing system must be appropriately chosen. Programmable System-on-chip (PSoC) is a technology that replaces the traditional ASIC (Application Specific Integrated Circuit) by an FPGA (known as Programmable Logics) combined with an Embedded Processor (known as the Processing system), integrated memories, a variety of peripherals to form an embedded computing system. The Programmable Logic is ideal for implementing high-speed logic, arithmetic and accelerating subsystems while the Processing System supports software routines and Operating systems. Based on this property, an algorithm can be partitioned into submodules to be co-processed by the hardware-software combination.

The goal of this research is to partition and profile a Star Recognition Algorithm then implement these modules on both the Processing System (Software) and the Programmable Logics (Hardware) to analyze the Algorithm implementation regarding Performance, Area of Implementation, Power Consumption.

Keywords: Star tracker, Star pattern recognition, Star recognition, Algorithms, Attitude determination, Embedded System, Programmable System on Chip (PSoC).

Acknowledgements

There are many people I want to thank for helping me in completing this work. Foremost, I would express my sincerest gratitude to my supervisor, Asst. Prof. Chen Shoushun for supporting and guiding me through my work and study with his knowledge and patience. I am very grateful for his insights and instructions in the hardware design for FPGA.

Many thanks to all my labmates of Satellite Research Center II, especially MEHTA Deval Samirbhai and Chin Shi Tong for the first steps of my research and the help whenever I am in troubles and doubt.

I would also like to thank Mrs. Janet Tan and Mrs. Pamela Ng, the technicians of Satellite Research Center II for helping me with all the lab facilities instructions also, setting up the equipment and providing resources whenever I need.

Finally, I sincerely thankful to my parents, my brother and all of my friends for their love and support throughout my study.

Contents

| | |
|---------------------------------------------------------------------|-------------|
| Statement of Originality | i |
| Supervisor Declaration Statement | ii |
| Abstract | iii |
| Acknowledgements | iv |
| List of Tables | vii |
| List of Figures | viii |
| 1 Introduction | 1 |
| 1.1 Overview and Motivations | 1 |
| 1.1.1 Introduction to spacecraft attitude determination | 2 |
| 1.1.2 Star Tracker for attitude determination approach | 2 |
| 1.2 Objectives | 4 |
| 1.3 Major contributions | 4 |
| 1.4 Organization of the thesis | 5 |
| 2 Literature Review | 6 |
| 2.1 Star Tracker Operations | 6 |
| 2.2 Centroiding Algorithm | 7 |
| 2.3 Liebe Star Recognition Algorithm | 10 |
| 2.4 Pyramid Star Recognition Algorithm | 12 |
| 2.5 Geometric Voting algorithm | 14 |
| 2.6 Star Identification Algorithm with Optimized database | 15 |

| | | |
|----------|----------------------------------------------------------------------------|-----------|
| 3 | Hardware and Software Co-processing Implementation of the Algorithm | 18 |
| 3.1 | Overview | 18 |
| 3.1.1 | FPGA - Programmable Logic - IP Block | 18 |
| 3.1.2 | System-on-a-chip | 22 |
| 3.2 | Partition and Profiling | 24 |
| 3.2.1 | Partition | 24 |
| 3.2.2 | Profiling | 26 |
| 3.2.3 | Partitioning and profiling results | 27 |
| 3.3 | Module implementation | 28 |
| 3.3.1 | Centroiding | 28 |
| 3.3.1.1 | Thresholding | 28 |
| 3.3.1.2 | The connected-components problem in centroiding | 30 |
| 3.3.1.3 | The one-pass scan algorithm | 31 |
| 3.3.1.4 | IP core design for the one-pass scan algorithm | 35 |
| 3.3.2 | Choose the reference star | 37 |
| 3.3.3 | Find the star pattern | 40 |
| 3.3.4 | Pattern searching | 40 |
| 4 | Experimental Results | 43 |
| 4.1 | Star data analysis | 43 |
| 4.2 | Hardware design | 45 |
| 4.2.1 | Components and Design Flow | 45 |
| 4.2.2 | Power Analysis | 47 |
| 4.3 | Runtime experiments | 49 |
| 4.3.1 | 512x512 dataset | 49 |
| 4.3.2 | 1024x1024 dataset | 52 |
| 4.3.3 | Runtime Comparison | 55 |
| 5 | Summary and Future Works | 57 |
| 5.1 | Summary | 57 |
| 5.2 | Future Works | 57 |
| | Bibliography | 59 |

List of Tables

| | | |
|-----|------------------------------------------------------------------------|----|
| 1.1 | Attitude determination accuracy comparison | 3 |
| 2.1 | A list of star centroids in an image | 9 |
| 2.2 | An example of Liebe star pattern database | 11 |
| 2.3 | A Pyramid star pattern example | 13 |
| 4.1 | Hardware resource consumption | 47 |
| 4.2 | Environment condition | 47 |
| 4.3 | Star tracker configuration | 49 |
| 4.4 | Software runtime | 50 |
| 4.5 | Hardware - Software Co-processing runtime | 51 |
| 4.6 | Specifications of the SST-20S star tracker and the real image[1] . . . | 52 |
| 4.7 | Software runtime | 53 |
| 4.8 | Hardware - Software Co-processing runtime | 54 |
| 4.9 | Runtime comparison | 56 |

List of Figures

| | | |
|------|------------------------------------------------------------------------|----|
| 1.1 | Star tracker hardwares | 3 |
| 1.2 | Commercial star trackers | 3 |
| 2.1 | Stages of star tracking algorithm | 7 |
| 2.2 | Stars projection onto a 2D image plane | 8 |
| 2.3 | Centroid of stars in an image | 8 |
| 2.4 | Star clusters represented in a 2D image plane | 9 |
| 2.5 | Liebe star pattern | 11 |
| 2.6 | Pyramid star pattern | 12 |
| 2.7 | Geometric Voting star pattern | 14 |
| 2.8 | Star Identification Algorithm with Optimized database star pattern . | 16 |
| 2.9 | A star pattern database tree-styled structure | 17 |
| 3.1 | A 4-input logic implemented by a Look up table (LUT)[2] | 19 |
| 3.2 | FPGA Routing Architecture[2] | 20 |
| 3.3 | FPGA Development Process Design Flow[2] | 20 |
| 3.4 | Xilinx Spartan-3AN Family Architecture[3] | 22 |
| 3.5 | An ASIC board | 23 |
| 3.6 | PS and PL connected through AXI | 24 |
| 3.7 | A Zedboard Programmable System on Chip | 25 |
| 3.8 | Module partitioning[4] | 26 |
| 3.9 | Profiling steps | 27 |
| 3.10 | Star tracking algorithm submodules partitioned. | 27 |
| 3.11 | Profiling result. | 28 |
| 3.12 | Thresholding separates star cluster pixels and background pixels . . . | 29 |
| 3.13 | Clustering pixel values | 30 |
| 3.14 | Star clusters represented as a connected-components problem | 31 |

| | | |
|------|------------------------------------------------------------------------|----|
| 3.15 | Left and above pixels of the current considering pixel. | 32 |
| 3.16 | one-pass scan algorithm applied to label 2-star clusters - 1 | 33 |
| 3.17 | one-pass scan algorithm applied to label 2-star clusters - 2 | 33 |
| 3.18 | one-pass scan algorithm applied to label 2-star clusters - 3 | 34 |
| 3.19 | one-pass scan algorithm applied to label 2-star clusters - 4 | 34 |
| 3.20 | one-pass scan algorithm applied to label 2-star clusters - 5 | 35 |
| 3.21 | IP core design purpose | 36 |
| 3.22 | Stream an image into a pixel stream | 36 |
| 3.23 | IP core submodules | 37 |
| 3.24 | Get above and left pixel functions | 37 |
| 3.25 | Stream processing submodule | 38 |
| 3.26 | centroid calculating submodule | 38 |
| 3.27 | The complete IP core module | 39 |
| 3.28 | Distances from the centre of the image to all stars | 39 |
| 3.29 | Distances from the reference star to its neighbors | 40 |
| 3.30 | Star pattern matching | 41 |
| 3.31 | Star pattern matching with tolerance | 42 |
| 4.1 | Number of stars in one image distribution | 44 |
| 4.2 | Star area distribution | 44 |
| 4.3 | Hardware design diagram | 45 |
| 4.4 | Hardware design block | 46 |
| 4.5 | Power consumption summary | 48 |
| 4.6 | Power consumption by components | 48 |
| 4.7 | Software runtime | 50 |
| 4.8 | Software - Hardware co-processing runtime | 52 |
| 4.9 | Software runtime | 54 |
| 4.10 | Hardware - Software Co-processing runtime | 55 |
| 4.11 | Runtime comparison | 56 |

Chapter 1

Introduction

1.1 Overview and Motivations

Artificial satellites orbiting the earth are a critical component of modern society. They are used in areas such as communication, positioning, imaging and weather forecasting. Besides the ordinary purposes of satellites like Earth observation, communication, weather forecasting[5], we also use satellites for research purposes. An example of this is the International Space Station (ISS) and the Hubble telescope.

Satellites operate in different orbits. Some popular orbit classes are Low Earth Orbit (LEO), Medium Earth Orbit (MEO) and High Earth Orbit (HEO)[6]. Low Earth Orbit is the area below 2000km, High Earth Orbit is the orbit above 35,500 km, and Medium Earth Orbit is the area between Low Earth Orbit and High Earth Orbit. Satellites are launched to their orbit by a self-propelled rocket as a piggyback payload.

Nanosatellite is a small artificial satellite with a wet mass(the total mass of the hardware plus fuel and oxidizer) between 1 - 10 kg. Nanosatellites are cheap but capable of performing commercial missions and has led researchers and scientists to explore the new way to use the Nanosatellites in LEO[7]. Their designs are only comprised of low-cost components. Due to their cost-effective, fast development cycle and size convenience, Nanosatellites are becoming popular in educational and scientific development. Nanosatellites can be quickly built in a small university project.

A satellite needs an attitude determination system for navigation and acknowledging orientations. Its attitude needs to be calculated and predicted continuously during its operation on the orbit. By observing the celestial objects and properties around the satellite, the satellite can autonomously estimate the orientations. Some of the favorite reference objects are the Sun, the Earth magnetic field, the celestial sphere, and the stars. For Nanosatellites, the attitude determination system must be concise but operate effectively.

1.1.1 Introduction to spacecraft attitude determination

Based on the celestial reference objects, many attitude determination sensors have been developed. Some of the sensors are the sun sensor, magnetometer, gyroscope, Earth horizon sensor[8]. The sun sensor is the most common sensor to be mounted on Nanosatellites due to its low cost, low power consumption, and lightweight. The sun sensor is also integrated with an Inertial Measurement Unit (IMU) which is capable of measuring the magnetic field, rotational speed and acceleration or a GPS to provide satellites position and velocity vector. The only disadvantage of the sun sensor is that its accuracy can only reach 1 arcminute resolution while the attitude determination system need a higher efficiency up to arc seconds resolution[9].

1.1.2 Star Tracker for attitude determination approach

Another way of attitude determination approach is using star trackers[10]. Star Tracker is an optical-electronics subsystem comprises of a CCD or CMOS Image sensor attached to an optical lens and a computing system, usually a microprocessor integrated into an ASIC board. The image sensor will firstly take an image of multiple star clusters at a specific fixed orientation. After that, the image is processed through the computing system to extract a particular feature of the model depending on a predefined algorithm. Then, the specific feature is compared with a prebuilt pattern or feature database stored in the memory. The output of the algorithm is often a star ID, which has a specific attitude, this attitude is again used to determine the attitude(orientation) of the spacecraft.



Figure 1.1: Star tracker hardware



Figure 1.2: Commercial star trackers

The star tracker is a preferred attitude determination approach because of its high accuracy compared to other sensors[11]. However, the star tracker approach is high cost and more power consumption than the traditional approach by sun sensor and IMU. To achieve the best accuracy, the star tracker depends on the many factors such as the quality of the image sensor, the quality of the optical lens, and most importantly the processing time of the computing subsystem, and the runtime of the star tracking Algorithm.

Table 1.1 depicts the accuracy comparison between star reference object and other celestial objects for attitude determination[10].

Table 1.1: Attitude determination accuracy comparison

| Reference Object | Potential Accuracy |
|------------------|--------------------|
| Stars | 1 arcsecond |
| Sun | 1 arcminute |
| Earth(Horizon) | 6 arcminutes |
| RF beacon | 1 arcminute |
| Magnetometer | 30 arcminutes |

1.2 Objectives

The essential goals of this research project are as followed.

- To analyze several star tracking algorithms especially in Lost in space (LIS) mode, the state that the spacecraft first time entering the orbit without any knowledge about its prior orientations compared to Tracking mode which is the state that the star tracker has been operating for a while, and its current orientations can be computed based on the prior information.
- To implement and evaluate the performance of a star tracking algorithm on specific hardware using hardware and software co-processing approach.
- To benchmark and optimize the algorithm in terms of the power consumption and the area of transistor implementation.

1.3 Major contributions

The major contributions of this research project are summarized as follows:

- First, we review three classic star tracking algorithms which are applying in commercial star trackers. Analyzing and comparing their strengths and weaknesses. We then discuss the novel star tracking algorithm presented in “An Autonomous Star Recognition Algorithm with Optimized Star Catalogue for Fast Search Performance” by M.D. Pham, K.S. Low and S.H. Chen[12, 13], introduce the steps of the algorithm and explain why the algorithm is suitable for applying in nano-satellites compared to the three classic star tracking algorithms and chosen to be implemented by the hardware-software co-processing approach.
- Based on the algorithm analysis, we partition the algorithm into submodules and propose which part should be implemented on the software part or the hardware part. Our main contribute includes (a) an optimized star tracking algorithm for hardware-software co-processing approach, (b) a star tracking embedded system for nano-satellites.

1.4 Organization of the thesis

The rest of the thesis is organized as followed:

- Chapter 2: Introduces the basis of star tracking operation, reviews some of the state of the art star tracking algorithms and the chosen algorithm to be implemented by the software-hardware co-processing approach.
- Chapter 3: Introduces and analyzes a proposed algorithm to be implemented on the hardware.
- Chapter 4: Discusses the result of the implementation regarding runtime performance and hardware resources.
- Chapter 5: Summarizes the work and proposes future research topics.

Chapter 2

Literature Review

2.1 Star Tracker Operations

The star tracking algorithm operates mainly in 2 different modes: the Lost in Space (LIS) and Tracking modes:

- LIS mode: the initial attitude is unknown, the star tracker must determine it which is the most critical part of the star tracking operation. LIS mode is operated at the time when the power system is switched on or reset after an attitude determination attempt if tracking mode failed[12].
- Tracking mode: after the initial attitude is recognized. The star tracker is switched to the Tracking mode. With the initial is acknowledged, the computing can easily predict and track the attitude based on the previous information.

On this research topic, we will only focus on the LIS mode operation. The LIS mode operation of a star tracker is generalized in Figure 2.1 which includes 3 main algorithms:

- Centroiding Algorithm: Perform an image preprocessing, the input is a star image captured from the image sensor processed to an output which are the coordinates of all star clusters presented in the image.
- Star Recognition Algorithm: The main part of LIS mode. The coordinates of the stars will be used to calculate a feature vector depending on a specific Star Algorithm. A Star Pattern Database (SPD) is also prebuilt from the

SAO catalog (Smithsonian Astrophysical Observatory Star Catalog) based on the specific pattern of the Star Algorithm and stored into the memory of the processing system for comparison and pattern recognition[13]. Then, the feature vector will be looked up and matched to an entry in the SPD. The entry will return a star ID which is an identification of a star presenting in the star image.

- **Attitude Determination stage:** The final stage of star tracking algorithm operated in LIS mode. The Star ID will be looked up again in the SAO catalog to extract the information about its attitude. Then a group of star attitude is used to calculate the attitude of the satellite. Some of the well-known Attitude Determination methods are the QUEST and TRIAD.

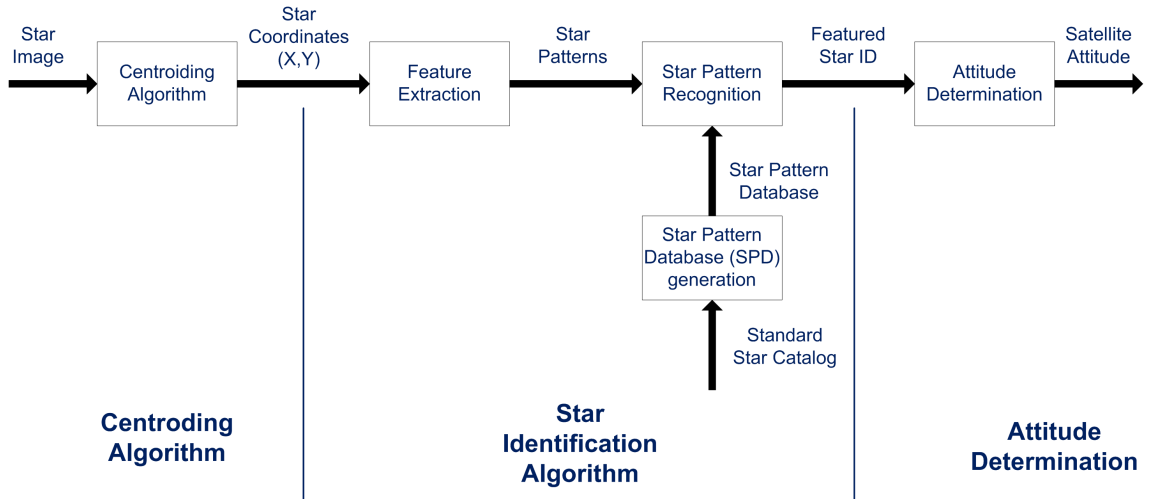


Figure 2.1: Stages of star tracking algorithm

This research topic will focus on the Centroiding and Star Identification Algorithm to be implemented on a computing system.

2.2 Centroiding Algorithm

The first step is to acquire the image which is accomplished by the image sensor. The image acquired has to be processed for estimating the coordinates of the stars in the image plane as shown in Figure 2.2. This is completed by applying the centroiding

process on the image. The input of this step is a star image with multiple star clusters. The output is the coordinate of every star presenting. Due to distributed energy surface, a star projection is spread over a 3x3 to 11x11 square area[14], and the star projection is a group of connected pixels. Therefore, the best way to identify the star clusters is to apply the connected component algorithm.

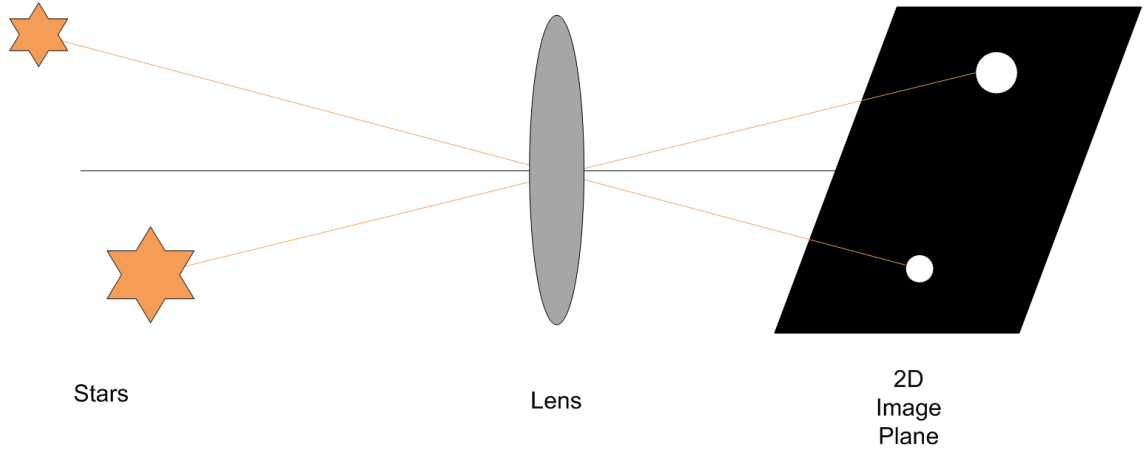


Figure 2.2: Stars projection onto a 2D image plane

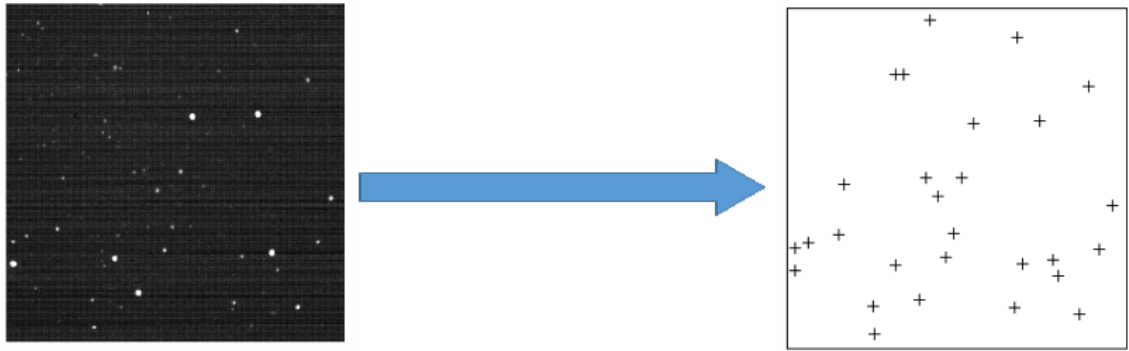


Figure 2.3: Centroid of stars in an image

Table 2.1 shows how star centroids in an image, as in Figure 2.3 are stored under a list of Cartesian coordinates. Besides, star trackers may use other coordinate systems like the Polar coordinate system, Cylindrical or Spherical coordinate systems.

A star pattern is spread over an area so we can calculate its centroid by applying

Table 2.1: A list of star centroids in an image

| Star | Coordinates(X,Y) |
|--------|------------------|
| Star 1 | (X_1, Y_1) |
| Star 2 | (X_1, Y_1) |
| ... | ... |
| Star N | (X_N, Y_N) |

the weighted pixel intensity technique. Equation 2.1 shows how to calculate a star centroid in Cartesian coordinate. Assume that (x, y) is the horizontal and vertical centroid coordinate of a star cluster, I_{ij} is each pixel intensity of the star pattern, i and j are the horizontal and vertical coordinates of each pixel within this star cluster.

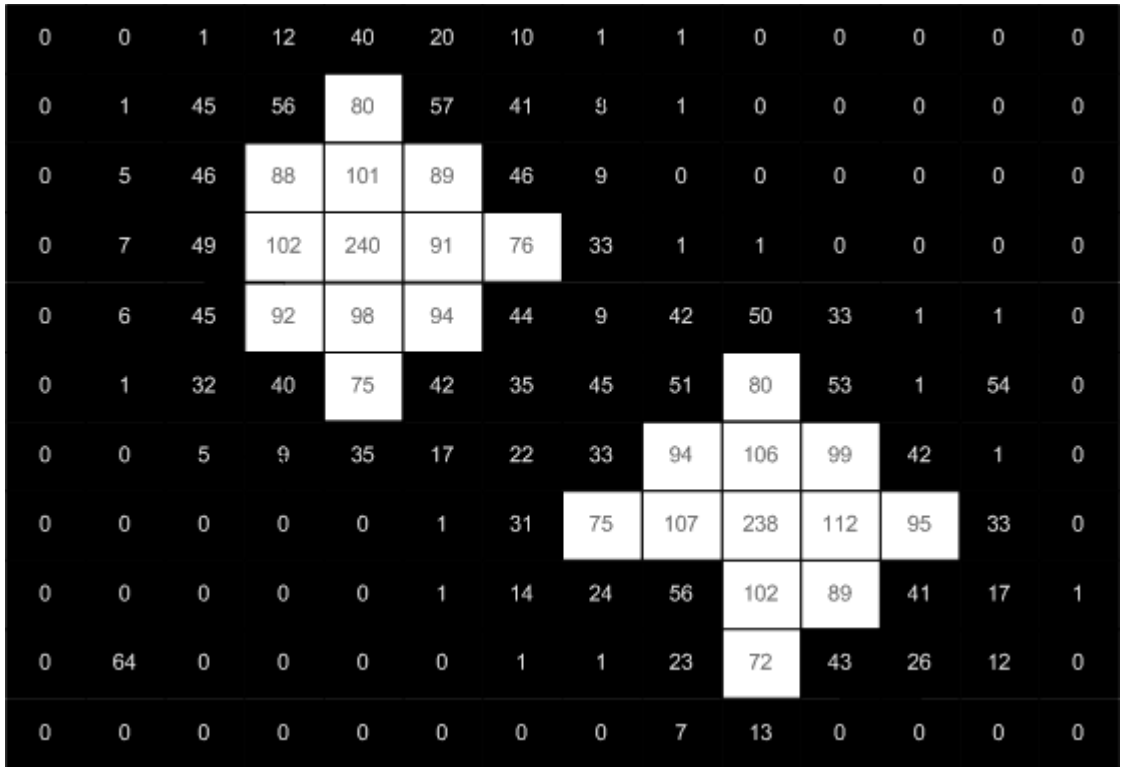


Figure 2.4: Star clusters represented in a 2D image plane

$$x = \frac{\sum_{i=1}^n \sum_{j=1}^m (i * I_{ij})}{\sum_{i=1}^n \sum_{j=1}^m I_{ij}}, y = \frac{\sum_{i=1}^n \sum_{j=1}^m (j * I_{ij})}{\sum_{i=1}^n \sum_{j=1}^m I_{ij}} \quad (2.1)$$

2.3 Liebe Star Recognition Algorithm

The star pattern recognition algorithm based on the angular features formed by a star triplet was reported in [10, 15–18]. The idea of Liebe Algorithm is to utilize 3 nearest-to-the centre stars. The closest-to-the-centre star is chosen as the reference star which will then return the star ID for Attitude Determination stage. Then the next 2 stars are chosen from the neighboring stars of the reference star which have the minimum and the second minimum distance to it.

The star triplet will form 2 angular distances θ_1, θ_2 and 1 angular angle θ which are defined by Equation 2.2. V_A, V_B, V_C are the Euclidean vectors connecting each star in the star triplet with the star tracker (or the spacecraft), V_{AB} is the Euclidean vector connecting star A and star B. Therefore, we have the Euclidean vector connecting star A and star C denoted by V_{AC} .

$$\begin{aligned} \theta_1 &= \cos(V_A, V_B) \\ \theta_2 &= \cos(V_A, V_C) \\ \theta &= \cos(V_{AB}, V_{AC}) \end{aligned} \quad (2.2)$$

In which A is the reference star. B and C are the 2 stars which are closest to A.

The feature vector of the Liebe star recognition algorithm is defined as Equation 2.3.

$$f = \{\theta_1, \theta_2, \theta\} \quad (2.3)$$

Table 2.2 shows an example of Liebe star pattern database. Each feature vector $f = \{\theta_1, \theta_2, \theta\}$ would return a corresponding star ID which identify the identification of the reference star. Thus, The table is sorted for quick searching purpose.

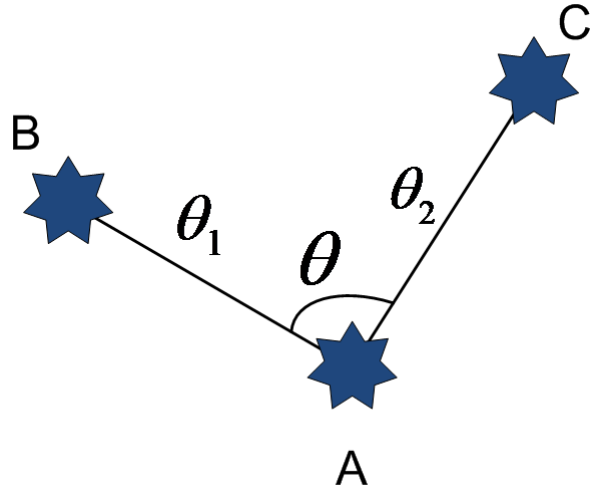


Figure 2.5: Liebe star pattern

Table 2.2: An example of Liebe star pattern database

| θ_1 | θ_2 | θ | Star ID |
|------------|------------|----------|---------|
| 54 | 80 | 32 | 55 |
| 54 | 80 | 33 | 631 |
| 54 | 81 | 32 | 114 |
| 54 | 81 | 33 | 1297 |
| 54 | 82 | 32 | 611 |
| 54 | 82 | 33 | 168 |
| 55 | 80 | 32 | 284 |
| 55 | 80 | 33 | 811 |
| 55 | 81 | 32 | 1289 |
| 55 | 81 | 33 | 6 |
| 55 | 82 | 32 | 602 |
| 55 | 82 | 33 | 1165 |
| 56 | 80 | 32 | 222 |
| 56 | 80 | 33 | 327 |
| 56 | 81 | 32 | 470 |
| 56 | 81 | 33 | 104 |
| 56 | 82 | 32 | 1058 |
| 56 | 82 | 33 | 1222 |

The most advantage of Liebe star recognition algorithm is that it is straightforward in implementation. It requires very few computations in the process.

The weakness of this algorithm is the weak robustness due to the limitation of star utilization. It only employs the three nearest stars to the centre and discards other stars which will then lead to a mismatch if the two predefined nearest neighboring stars do not appear in the star image. Besides, if the reference star appears in the final entry of the Star Pattern Database, the searching algorithm would fall into the worst case.

2.4 Pyramid Star Recognition Algorithm

To overcome the mismatches caused by lack of information employed by Liebe algorithm, the pyramid star recognition algorithm is proposed in[19–23]. Its searching pattern is a combination of angular distances of 4 stars in the star image. In Figure 2.6, the 4 stars: A,B,C,D is chosen to build the pattern. The reference star which is star A in the example is the closest star to the centre of the image. Next, the 3 neighboring stars around star A are selected to form a feature vector from the 4-star angular distances.

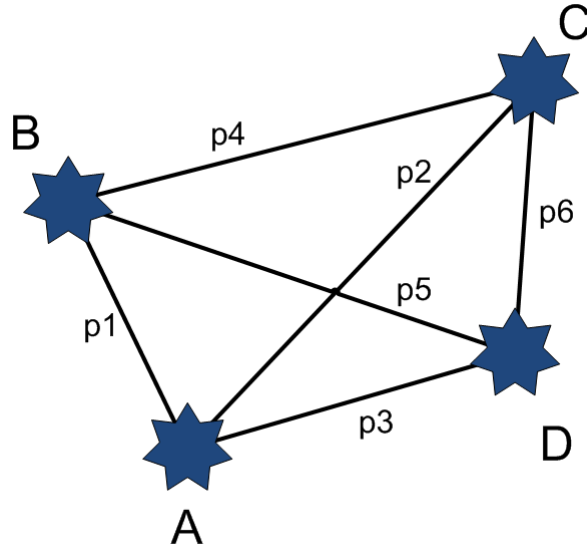


Figure 2.6: Pyramid star pattern

$$f = \{p_1, p_2, p_3, p_4, p_5, p_6\} \quad (2.4)$$

Table 2.3: A Pyramid star pattern example

| Angular distances | Star 1 | Star 2 |
|-------------------|--------|--------|
| p_1 | A | B |
| p_2 | A | C |
| p_3 | A | D |
| p_4 | B | C |
| p_5 | B | D |
| p_6 | C | D |

One of the advantages of the pyramid algorithm is that it employs 4 stars to build the feature vector compared to only 3 stars of the Liebe algorithm. Compared to Liebes, this method is more robust since it makes the star recognition process more accurate as six features (as denoted in Equation 2.4) are utilized for identification purpose compared to only three features used by the Liebe algorithm[24]. The Table 2.3 describes how the star patterns $p_1, p_2, p_3, p_4, p_5, p_6$ are defined by angular distances between Star 1 and Star 2.

However, in a tradeoff, more memory space is needed since it requires to store at least 6 pairs of each starID entry this will lead to increase the memory required to store the star pattern database and the processing time will be increased due to the increase in pattern storage and comparisons. The time complexity is also a significant consideration. To solve this problem, the k-vector search has been introduced in[21, 23]. The time complexity has been reduced significantly which is equivalent to the Liebe searching method.

Moreover, the pyramid star recognition algorithm has not yet solved the mismatch problem caused by missing stars. In the case of one or more neighboring stars of the reference are missing, the algorithm will fail and do not produce a correct result.

2.5 Geometric Voting algorithm

To overcome the weaknesses of Liebe and Pyramid star recognition algorithms, the Geometric Voting is proposed based on voting of radial distances[25]. The Geometric Voting method considers all the nearby stars of the reference star appeared in the star image. Thanks to all stars in the image are employed, the Pyramid algorithm becomes more robust than the first two algorithms.

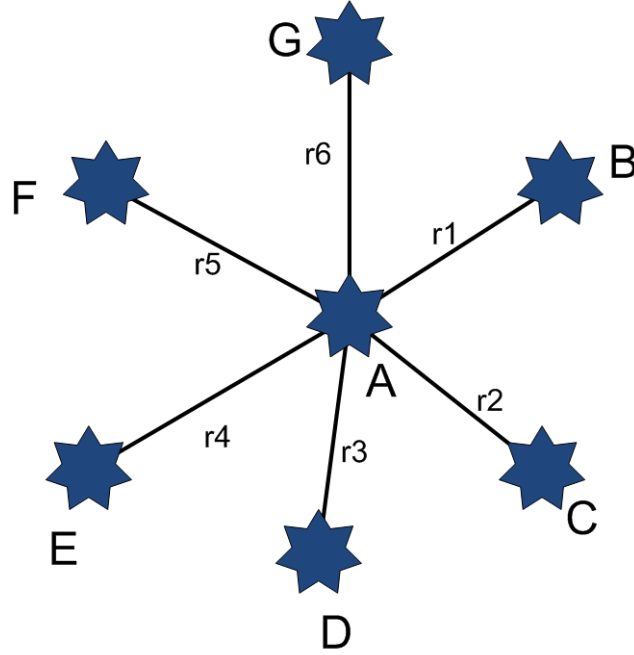


Figure 2.7: Geometric Voting star pattern

The feature vector is now not a fixed number of elements as in equation 2.5.

$$f = \{r_1, r_2, \dots, r_n\} \quad (2.5)$$

After capturing the image, r_1, r_2, \dots, r_n are calculated based on the distance from the closest star to the centre which is the reference star for all other stars within the Field of View(FOV) of the star sensor. Then all the distances from the feature vector are compared to the predefined neighboring distances of every star ID in the SPD. With each distance is matched, a voting value of the star ID is increased. After the comparing distance stage processed, the star ID which has the highest vote is recognized as the correct star ID candidate.

The advantage of this recognition method is that it employs all the data presenting in the image. As a result, it reduces the mismatching issued caused by lack of data proposed by Liebe and Pyramid method. Thus, it is the most robust star recognition method compared to the first two introduced methods.

The critical drawback of this method is the enormous space complexity needed to store the Star Pattern Database since each star ID entry must store the information of all of its neighboring stars. It leads to the requirement that a large memory must be used to store the Star Pattern Database to trade off of the accuracy and robustness. Thus, the processing time for returning a star ID is increasing due to the increase in data processing and comparisons through the whole database.

2.6 Star Identification Algorithm with Optimized database

In a quick review and analysis of the 3 prestigious and famous star recognition algorithms, we can come up with a conclusion that there is a trade-off between accuracy and robustness with the space complexity and processing time required. For the star tracker system, the choice of algorithm to be implemented on will depend on the scale of the satellite project. For military satellite, we favor the accuracy and robustness over the complexity of time and space. Thus, the computer system on those satellites must be fast enough to handle the complexity.

For the implementation on the nanosatellites, the computer system is a small embedded processor with limited memory and processing ability which can not handle a large number of computations. Therefore, we need an optimized algorithm that is accurate, robust and can be implemented on a small computer system.

The chosen star tracking algorithm is from the paper “An Autonomous Star Recognition Algorithm with Optimized Star Catalogue for Fast Search Performance” by M.D. Pham, K.S. Low and S.H. Chen[12,13]. The algorithm introduces a novel star pattern identification using an optimized database and proposes a search tree data structure for quick and advanced parallel search.

This star identification algorithm employs all the star appeared in the FOV like the geometric voting algorithm. The distances from the reference star to its neighboring stars are considered, and thus, another field is added to yield the star pattern, the number of stars appeared within the FOV of the star sensor.

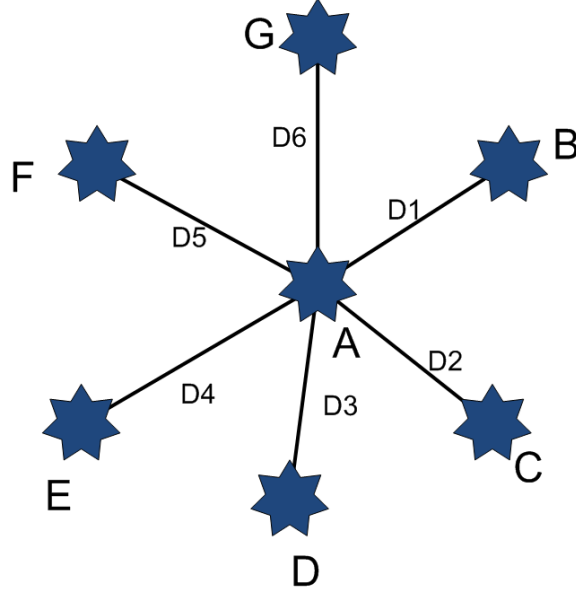


Figure 2.8: Star Identification Algorithm with Optimized database star pattern

The feature vector is described in Figure 2.8.

- N: Number of stars appeared within the FOV of the star sensor.
- $D_1, D_2, D_3, \dots, D_n$: Distances from the reference star to all of its neighbors.

To search and match the star pattern vector with the database, a special the tree structured database is pre-built. Figure 2.9 shows an example of this tree structured database. The tree is built with multiple levels, the first level is N-Number of stars in the FOV, next layers will be the distances from the reference stars to all of its neighbors which are sorted ascendingly from nearest neighboring star to the farthest.

In the searching and matching stage, each parameter from the star pattern is dispatched and matched to the equivalent level. If the matching succeeds, the next

layer is considered. If all layers are matched the correct star ID will be returned; otherwise, we return a statement that the star pattern is a false pattern, no stars were matched. In this case, depend on the attitude determination system on the satellite, the star identification algorithm would be rerun or skipped to proceed to the next star image.

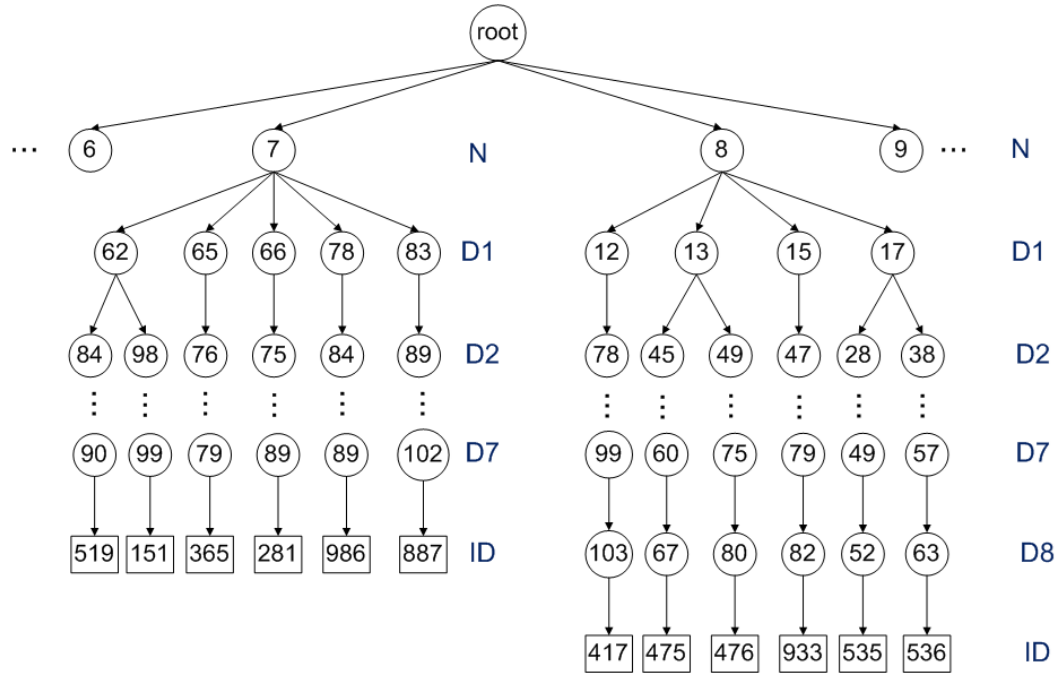


Figure 2.9: A star pattern database tree-styled structure

Chapter 3

Hardware and Software

Co-processing Implementation of the Algorithm

3.1 Overview

3.1.1 FPGA - Programmable Logic - IP Block

FPGA (Field Programmable Gate Array) provides a general purpose digital logic with great flexibility and utility. The fundamental logic cells of an FPGA work using look up tables (LUTs). The performance of an FPGA design depends on the area using and routing of LUTs[26].

LUTs: FPGAs were first designed to imitate Gate Arrays integrated circuits with a sea of gates that were connected by added metal layers (wire routing) to define the functionality of the device. However, instead of implementing the logic using transistor gates, the logic was in many cases implemented by memory fashioned as look up tables. Figure 3.1 shows an example of a Look up table implementing a 4-input logic function $F = (A \wedge B) \vee (C \wedge \bar{D})$. Instead of connecting the logic gates, the Lookup table memorizes the output result corresponding to the input combinations.

Routing: The routing in an FPGA is hierarchical. At the lowest level, we have a

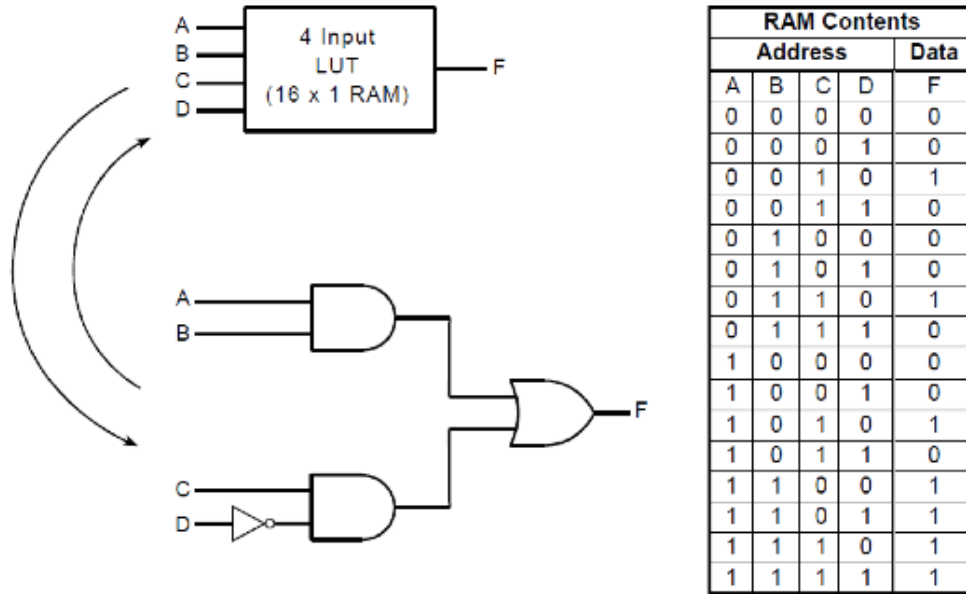


Figure 3.1: A 4-input logic implemented by a Look up table (LUT)[2]

routing switch that is controlled by a bit of SRAM, or a FLASH bit, or a fuse. There are many routing switches in the local routing to connect various logic elements or blocks. The FPGA is made of a sea of these logic blocks. Groups of the blocks are connected by long lines or very long lines. Common signals like clocks are routed on special routing networks called global networks. The FPGA routing architecture is demonstrated in Figure 3.2

FPGA design flow: The design begins with design entry, continues with simulation to verify the logic is implemented as expected, and then the tool will perform synthesis (also called mapping) to map the logic to the device architecture. Next the tool will create the interconnection between cells by placing and routing (or fitting) the design. Another simulation after the fitting is done is a good practice. If this looks good, the next step to use the tool to create a programming file, which is then downloaded into the FPGA device for testing[2]. The FPGA design flow is presented in Figure 3.3

Programmable Logic: In Xilinx architecture, the FPGA part of the design is called Programmable Logic (PL). Some of the specialized components in the architecture include:

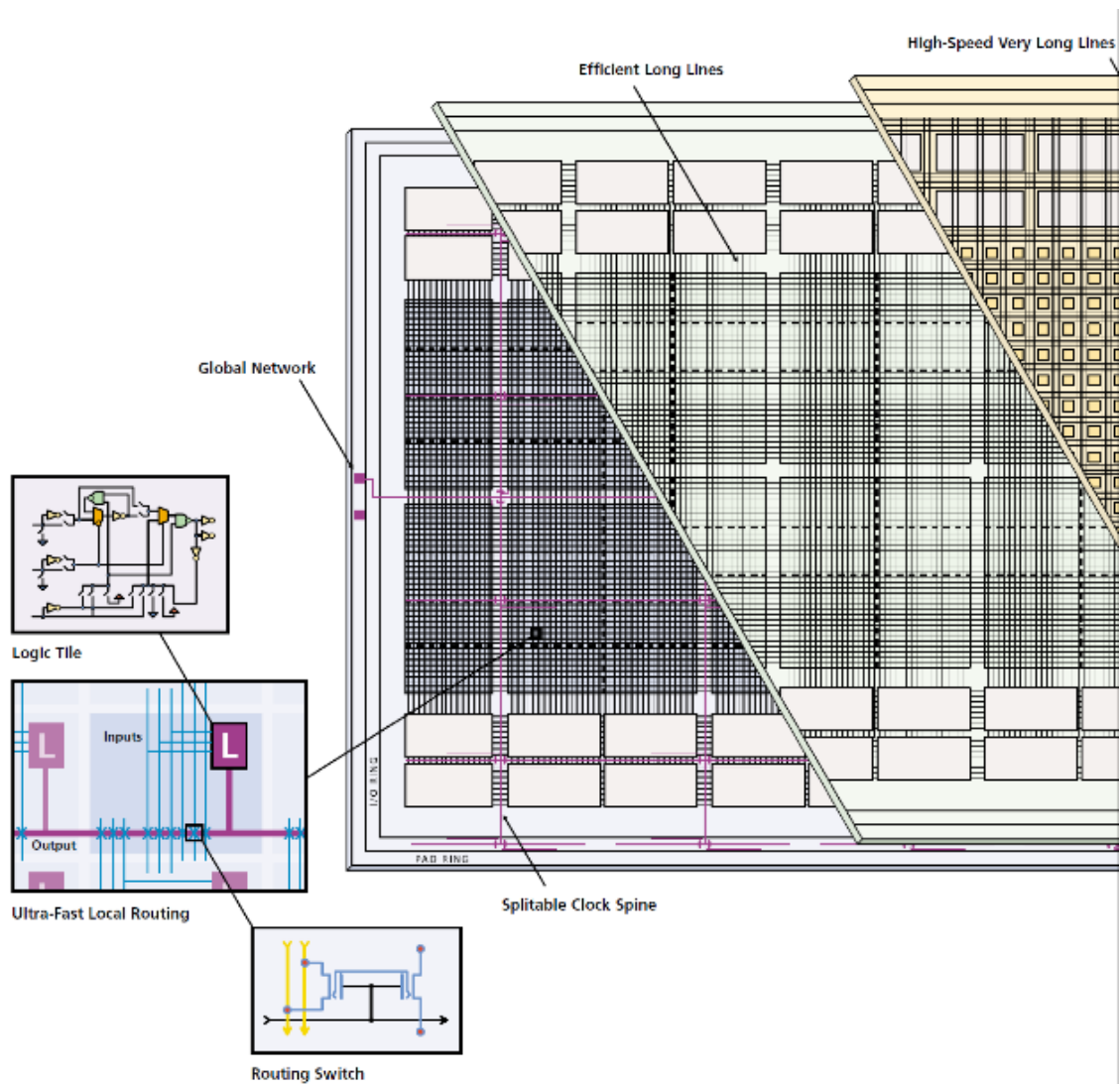


Figure 3.2: FPGA Routing Architecture[2]

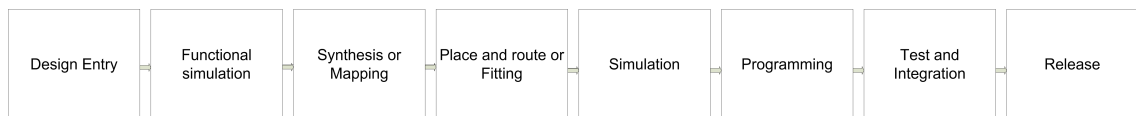


Figure 3.3: FPGA Development Process Design Flow[2]

- **Configurable Logic Blocks (CLBs)** contain flexible Look-Up Tables (LUTs) that implement logic plus storage elements used as flip-flops or latches.
- **Input/Output Blocks (IOBs)** control the flow of data between the I/O pins and the internal logic of the device. IOBs support bidirectional data flow plus 3-state operation. They support a variety of signal standards, including several high-performance differential standards. Double Data-Rate (DDR) registers are included.
- **Block RAM** provides data storage in the form of 18-Kbit dual-port blocks.
- **Multiplier Blocks** accept two 18-bit binary numbers as inputs and calculate the product.
- **Digital Clock Manager (DCM) Blocks** provide self-calibrating, fully digital solutions for distributing, delaying, multiplying, dividing, and phase-shifting clock signals.

These elements are organized as shown in Figure 3.4. A dual ring of staggered IOBs surrounds a regular array of CLBs. Each device has two columns of block RAM. Each RAM column consists of several 18-Kbit RAM blocks. Each block RAM is associated with a dedicated multiplier. The DCMs are positioned in the center with two at the top and two at the bottom of the device. The design has two DCMs in the middle of the two columns of block RAM and multipliers.

The Xilinx Programmable Logic features a rich network of traces that interconnect all five functional elements, transmitting signals among them. Each functional element has an associated switch matrix that permits multiple connections to the routing[3].

Intellectual property core, IP core, or IP block is a reusable unit of logic, cell, or integrated circuit (commonly called a "chip") layout design that is the intellectual property of one party. IP cores may be licensed to another party or can be owned and used by a single party alone. The term is derived from the licensing of the patent and/or source code copyright that exist in the design. IP cores can be used

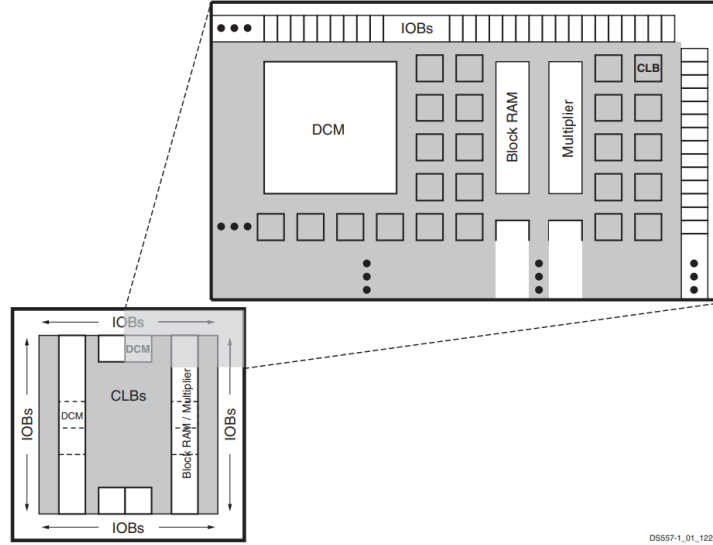


Figure 3.4: Xilinx Spartan-3AN Family Architecture[3]

as building blocks within application-specific integrated circuit (ASIC) designs or field-programmable gate array (FPGA) logic designs[27].

3.1.2 System-on-a-chip

System-on-a-chip (SoC) is anatomy in embedded system which considers a processing board integrated with processor and hardware peripherals and memory for a specific function like digital, analog signal processing[28].

Traditional SoC board is a fixed Application Specific Integrated Circuit (ASIC) (Figure 3.5) which is prebuilt for only one particular function or task. The processing time of ASIC board is fast and highly efficient due to the unique hardware prebuilt for this task. In the trade-off, the development time of an ASIC board takes much longer due to multiple stages of hardware synthesis, testing and verification and the cost of development is enormous. ASIC board is only suitable for mass-production strategy with over 1 million products per development cycle.

Another approach is using an embedded processor(Figure ??) for the implementation. All stages of the development are equivalent to a software development process. This approach brings some advantages like low-cost development, flexibility, easy to



Figure 3.5: An ASIC board

fix and testing, short-time-development, and short-time-to-market. On the downside, the approach of using multipurpose processors causes high power consumption, low efficiency in the product operation.

Programmable-System-on-a-chip (PSoC) is a hybrid way approach of SoC embedded system. It replaced the traditional ASIC by a Programmable Logic (FPGA) interfacing and embedded multipurpose processor with an integrated Processing system (usually a hard processor) through a high-speed bus. For zynq PSoC, the Advanced eXtensible Interface (AXI) is this high speed communicating bus. The PSoC cannot achieve the high-efficiency as the traditional ASIC approach but thanks to the modern technology and the short development time, the PSoC approach is the most suitable candidate for research and development projects which is below 1000 products for a cycle.

The PSoC board which is used to implement Star Tracking algorithm in this project is the Zynq zedboard illustrated in Figure 3.7. The defining feature of Zynq is that

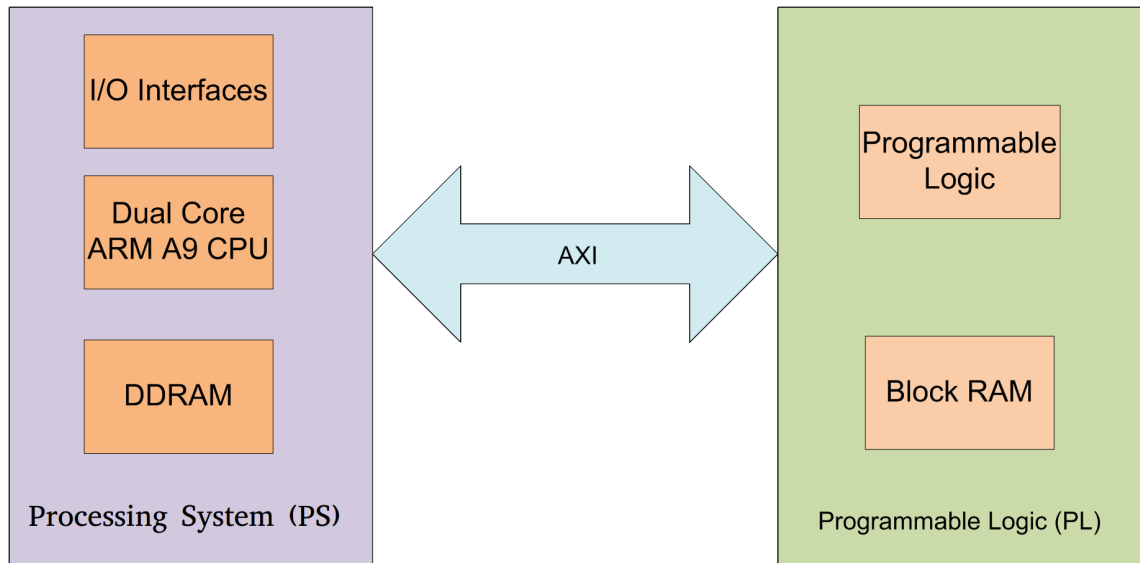


Figure 3.6: PS and PL connected through AXI

it combines a dual-core ARM-A9 processor with traditional FPGA logic fabric[29]. Although dedicated processors have been coupled with FPGAs before, it has never been quite the same proposition. In Zynq, the ARM Cortex-A9 is an application grade processor, capable of running full operating systems such as Linux, while the programmable logic is based on Xilinx 7-series FPGA architecture.

3.2 Partition and Profiling

3.2.1 Partition

Partitioning is the first stage of PSoC development. The algorithm or the program will be partitioned into suitable-size submodules. These submodules are later decided to be implemented on which side of the PSoC: Programmable Logics or Processing System as illustrated in Figure 3.8. How the program is partitioned, decided by the designer.

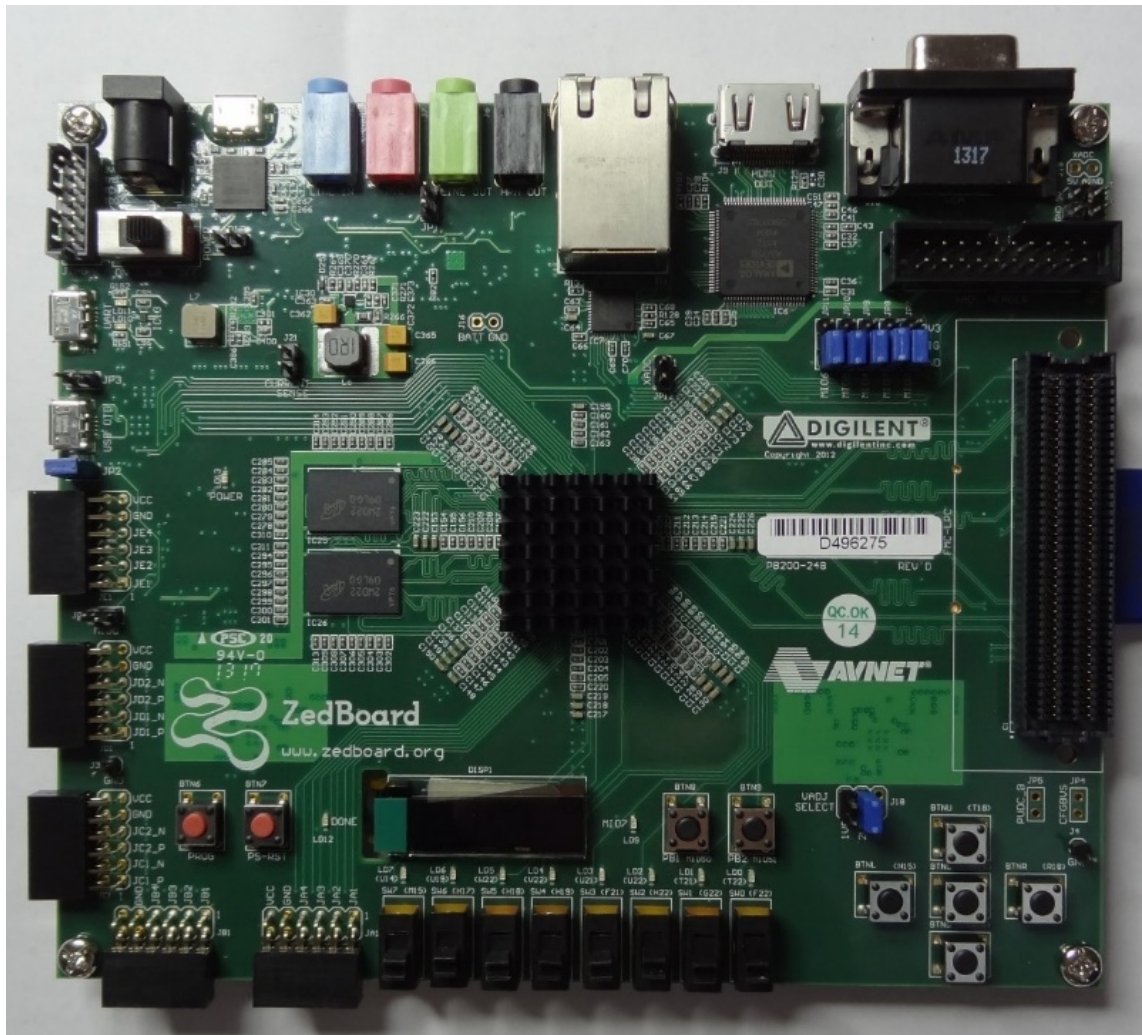


Figure 3.7: A Zedboard Programmable System on Chip

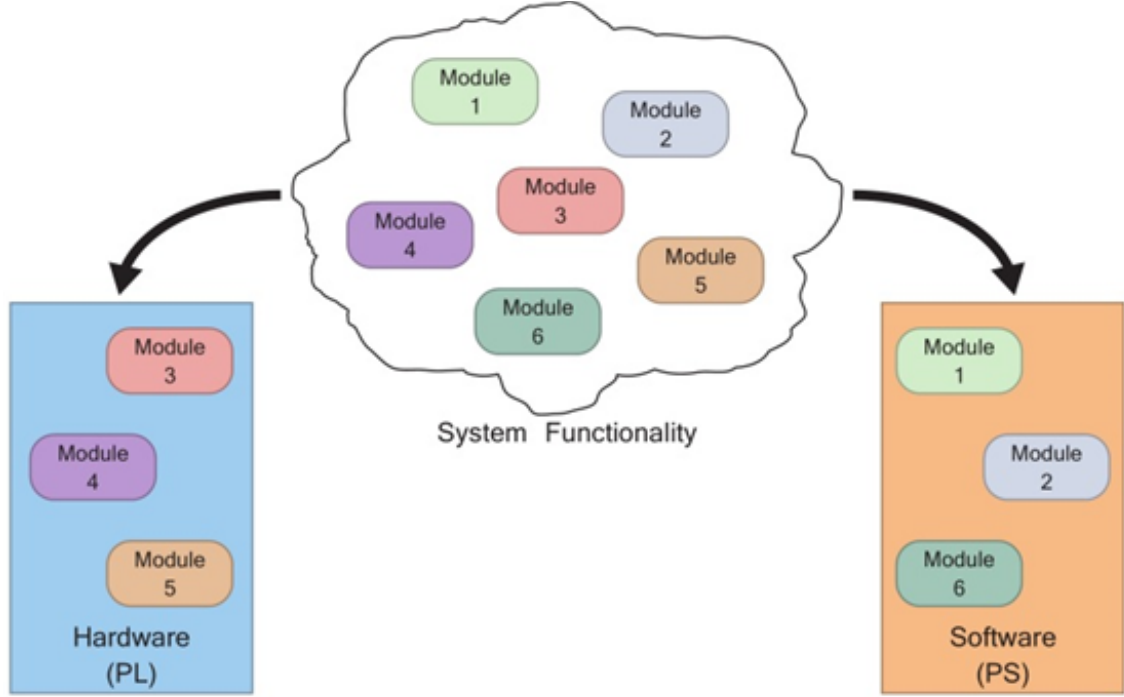


Figure 3.8: Module partitioning[4]

3.2.2 Profiling

Profiling is a practical analysis that measures and analyze the space and time complexity of an algorithm or a submodule of an algorithm. By examine the profiling result, we can specify the most critical time-consuming part or module of the system. Then based on the profiling and asymptotic analysis stated above, we can decide correctly which parts or submodules can be implemented in hardware instead of software. The profiling steps

All the submodules are implemented on Processing System side by software approach then determined which submodules take the most time to run. These modules then are optimized and designed as Intellectual Property core by Hardware description language (HDL) on Programmable Logics side.

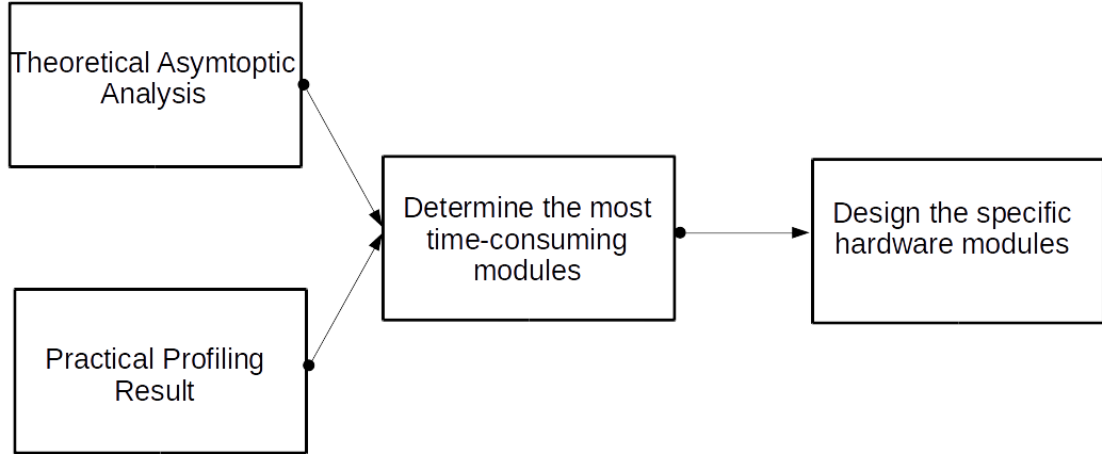


Figure 3.9: Profiling steps

3.2.3 Partitioning and profiling results

The star tracking algorithm is partitioned into 4 submodules as shown in Figure 3.10. The 4 submodules include:

- **Centroiding:** Takes the star image and reproduce the star coordinates in the image.
- **Choose the reference star:** From the list of star coordinates, proceeds to choose the reference star.
- **Find the star pattern:** From the reference star, generates the feature vector of the image.
- **Pattern searching:** Search and match the feature vector to the prebuilt tree database to get the starID of the reference star.



Figure 3.10: Star tracking algorithm submodules partitioned.

After partitioning, all submodules are implemented on the Processing system side to examine the runtime of each submodule. The result of profiling stage is shown

in Figure 3.11.

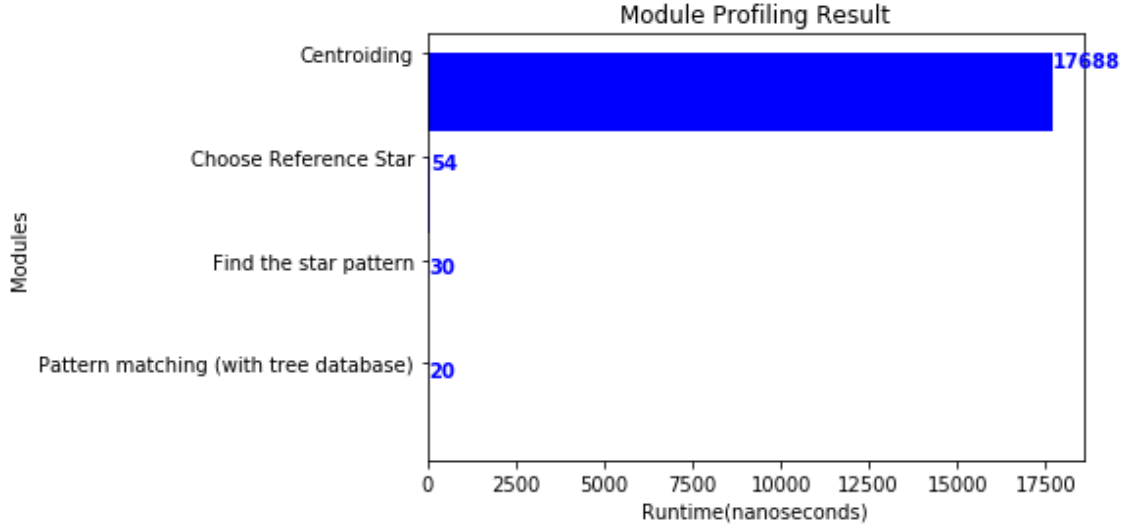


Figure 3.11: Profiling result.

Apparently, the most time-consuming submodule is the centroiding module. It can be explained because the centroiding stage is an image processing stage. Implementation of an image processing algorithm on general purpose processors is more costly and less effective than any other parallel processing approach like using a graphics processing unit (GPU), in this thesis, we design the centroiding module as an IP core in the Programmable Logic side instead.

3.3 Module implementation

3.3.1 Centroiding

3.3.1.1 Thresholding

In the first stage, the sky is captured by a Charge-coupled device(CCD) through lens then discretized into digital star images. In which, each pixel is an 8-bit integer value which represents the intensity or brightness of a pixel(0 represents darkest pixel and 255 represents the brightest pixel). The star image is usually contaminated with noise as a result of dark current noise and non-star stellar object. Dark current

noise arises from thermal energy within the silicon lattice. It can be represented as a background image generated by a certain period of exposure with the shutter closed[8]. To eliminate the noise and separate star clusters from the background, we apply thresholding technique. The threshold level can be chosen by the Average Pixel Intensity technique. The pixel which has a higher value than threshold level belongs to a star cluster while the pixel which has a lower value than the threshold belongs to the background. Figure 3.12 shows how to separate star clusters from the background.

Most of the star images are affected by noise. Sometimes, the star tracker misleads the noise as a star which often leads to a mismatch. Therefore, the threshold should be carefully chosen. If we set the threshold too low, it would lead to mismatches. Otherwise, if we set the threshold too high, some stars would be missing from the image.

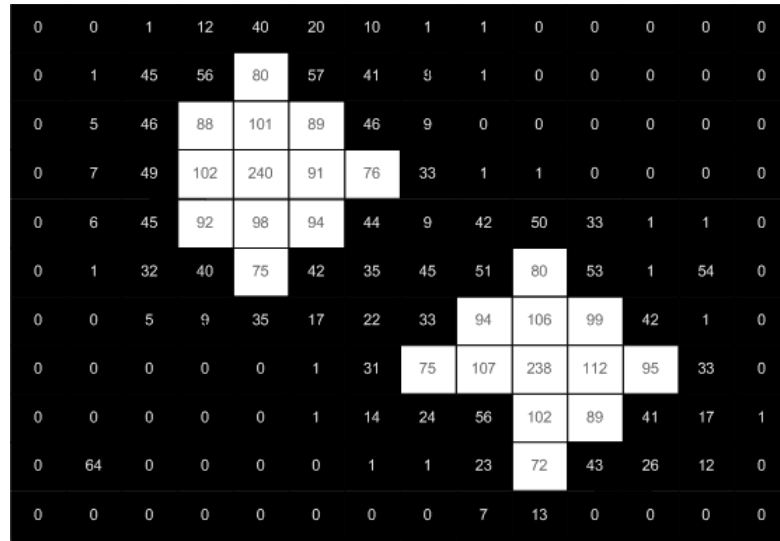


Figure 3.12: Thresholding separates star cluster pixels and background pixels

The Average Pixel Intensity technique is applied to choose the threshold value. Firstly, we perform an analysis by averaging and counting the occurrences of all the pixel values in the star image dataset. The pattern of the analysis is simulated as in Figure 3.13. It includes 2 significant clusters: the first cluster is the background pixel values which formed near 0 Intensity value and the second cluster is the star

pixel value which formed near the 255 Intensity value. There will be some scattered data points in between which represent the noise values. Based on the pattern we may know the range of the threshold value. To select the threshold value precisely, while running the algorithm on the test dataset, we fine-tune the threshold value again within the range to achieve the best accuracy. After performing the analysis and carrying out the algorithm on the test dataset, we choose the threshold value 70 which mostly produce high matching accuracy.



Figure 3.13: Clustering pixel values

3.3.1.2 The connected-components problem in centroiding

The raw image is contaminated with noises and other non-stellar objects. The noise can be canceled by setting a threshold level. If a pixel Intensity is less than the threshold level, we will set its value to 0(the background level) to differentiate from star cluster pattern. After all false star noise is canceled, the centroiding algorithm proceeds.

The technique to determine star centroids in a star image employs the connected component finding. The traditional approach of connected component finding is considering each pixel in the star image as a vertex in a graph. If a group of pixels belongs to a star cluster pattern, those vertices are connected. Therefore we can determine each independent star cluster by using a graph traversing technique like Depth-First-Search (DFS) or Bread-First-Search (BFS). However, this submodule of the star tracking algorithm is implemented as an IP core by Hardware Description Language (HDL) which lack abilities to implement a recursive function or advanced data structure like Queue and Stack.

The emergence of FPGAs with enough capacity to perform complex image processing tasks also led to high-performance architectures for connected component labeling[30]. Most of these architectures utilize the one-pass scan algorithm, because of the limited memory resources available on an FPGA. These types of connected component labeling architectures are able to process several image pixels in parallel, thereby enabling a high throughput at low processing latency to be achieved[31].

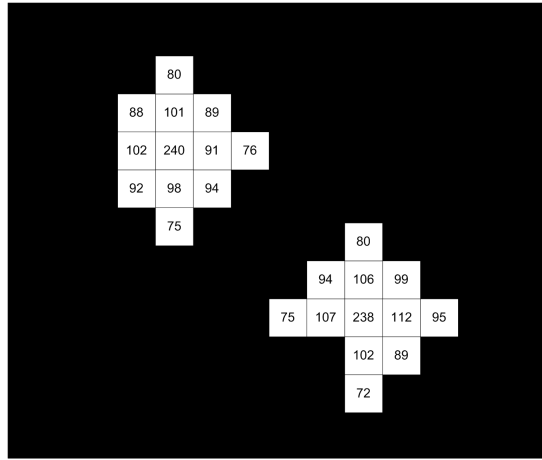


Figure 3.14: Star clusters represented as a connected-components problem

Figure 3.14 represents the star centroid finding problem as finding a connected-components problem. The same star cluster pixels are neighboring to each other. To determine the centroid of each star cluster, we must label the pixels into their corresponding star clusters(groups) then calculate each star cluster centroid of each cluster.

3.3.1.3 The one-pass scan algorithm

The one-pass scan algorithm is a connected component labeling approach which performs a scanning throughout the star image. Each star cluster is equivalent to each disjoint set. While scanning the picture, we try to identify which star pixel is corresponding to which disjoint set by applying the following rules.

If the pixel value is higher than the defined threshold which distinguish between the star pixel and the background of the image, we consider its left and above pixels as in Figure 3.15. There are 3 cases:

1. **Case 1 - Both are background pixels:** Label the pixel (P) with a new number. Create a new subset.
2. **Case 2 - One(either pixel) is labeled, the other is not or both are labeled with the same number:** Label the pixel (P) with this number.
3. **Case 3 - Both are labeled with different numbers:** Label the pixel (P) with any number from the left or above pixels, merge the set of the above pixel into the set of the left pixel.

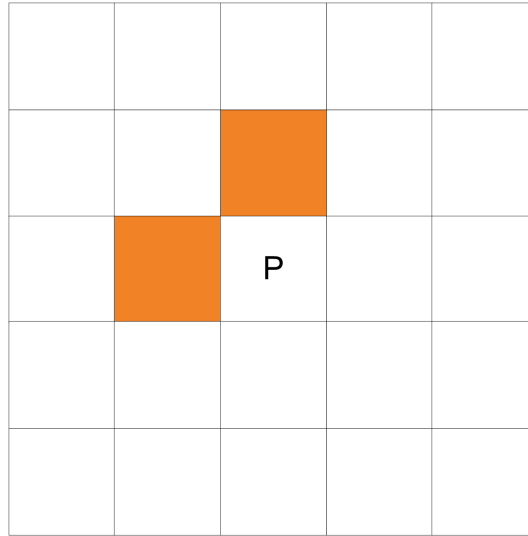


Figure 3.15: Left and above pixels of the current considering pixel.

An example of the one-pass scan algorithm applied to label 2-star clusters: In Figure 3.16, the first non-background pixel P has been scanned and comes into case 1(both left and above pixels are background pixels), so we create a new disjoint set(set 1) and add this pixel to set 1.

Next, we scan the pixel in Figure 3.17, the above pixel is a background pixel, and its left pixel is in set 1. Therefore, we apply case 2 of the algorithm, set this pixel to the same set as its left pixel which is set 1.

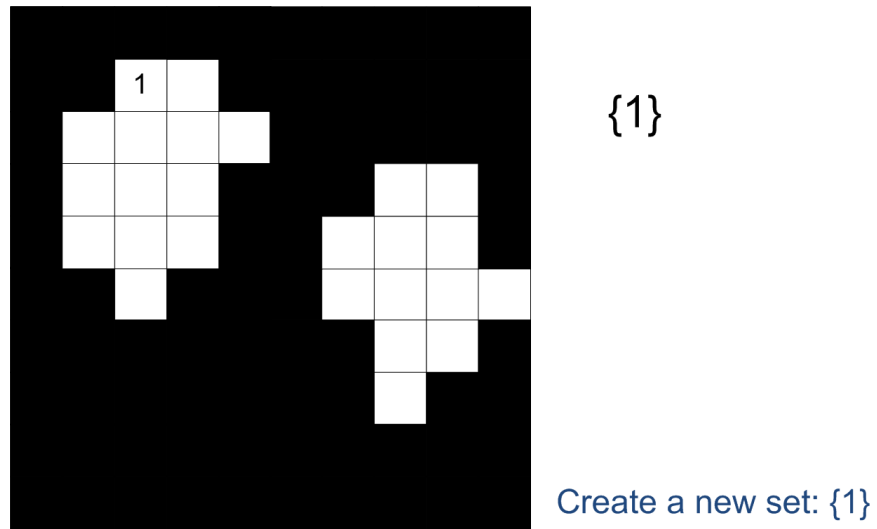


Figure 3.16: one-pass scan algorithm applied to label 2-star clusters - 1

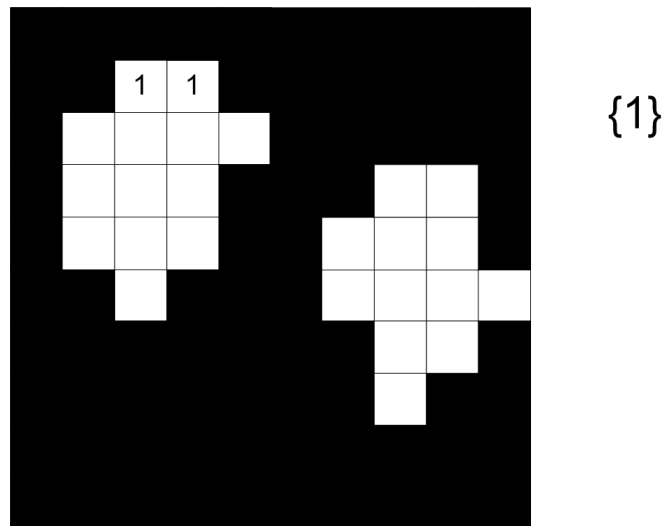


Figure 3.17: one-pass scan algorithm applied to label 2-star clusters - 2

After skipping background pixels, we consider the pixel shown in Figure 3.18, both above and left pixels of this pixel are background pixels(case 1). We create a new disjoint set(set 2) and add this pixel to set 2.

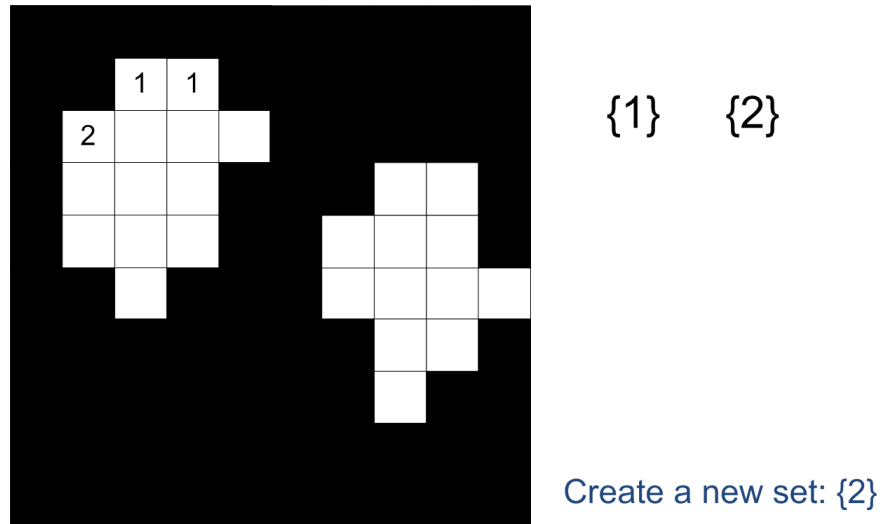


Figure 3.18: one-pass scan algorithm applied to label 2-star clusters - 3

The next pixel in Figure 3.19 belongs to case 3, so we merge 2 disjoint sets 1 and 2 and label this pixel as belonging to set 2.

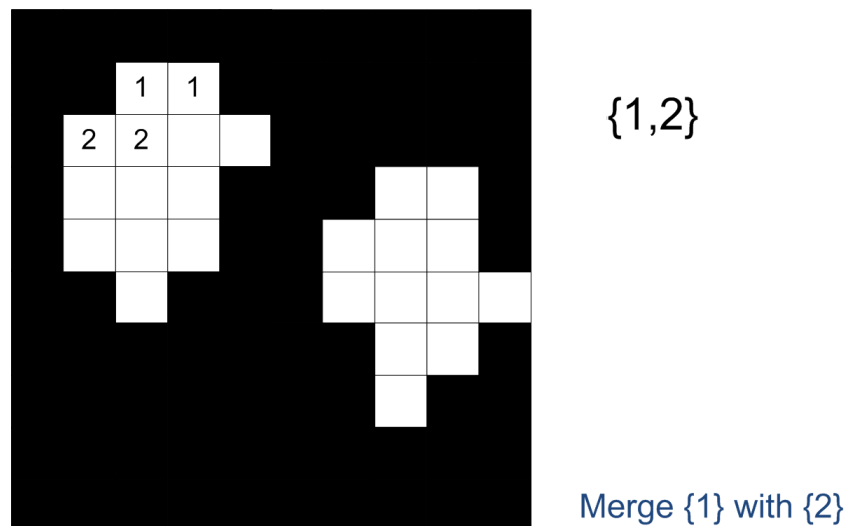


Figure 3.19: one-pass scan algorithm applied to label 2-star clusters - 4

At the final stage in Figure 3.20, we successfully find the 2 connected-component

which are the pixels belongs to set 1,2, and the pixels belongs to set 3,4.

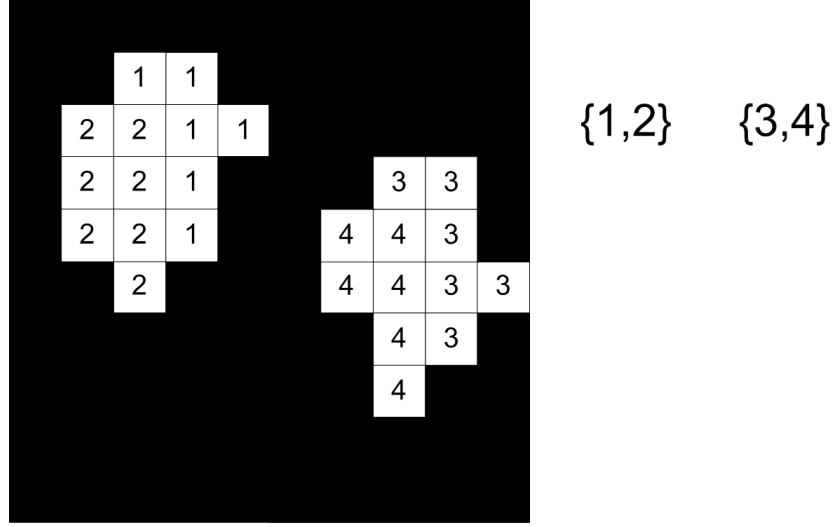


Figure 3.20: one-pass scan algorithm applied to label 2-star clusters - 5

After detecting the star clusters, we calculate the centroids of each star cluster by equation 3.1

$$x = \frac{\sum_{i=1}^n \sum_{j=1}^m (i * I_{ij})}{\sum_{i=1}^n \sum_{j=1}^m I_{ij}}, y = \frac{\sum_{i=1}^n \sum_{j=1}^m (j * I_{ij})}{\sum_{i=1}^n \sum_{j=1}^m I_{ij}} \quad (3.1)$$

The reason to choose the one-pass scan algorithm is that an image can not be loaded into the hardware processing unit as a matrix or tensor but as a pixel stream. We only know the previous pixels of the current receiving pixel.

3.3.1.4 IP core design for the one-pass scan algorithm

An image as streamed pixels

From the one-pass scan algorithm, we need to design an IP core for faster hardware processing. The input of the module is a stream of pixels, and the output is the centroid coordinates of the stars in this image as shown in Figure 3.21.

In figure 3.22, the pixel coordinates(i,j) in 2D images would be represented by the stream order(k). The reason we need to have a converting framework is that we need to look up the above and left pixels of the pixel in the one-pass scan algorithm.

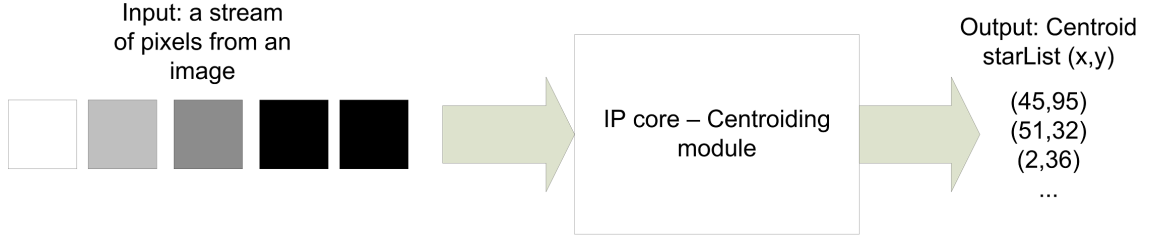


Figure 3.21: IP core design purpose

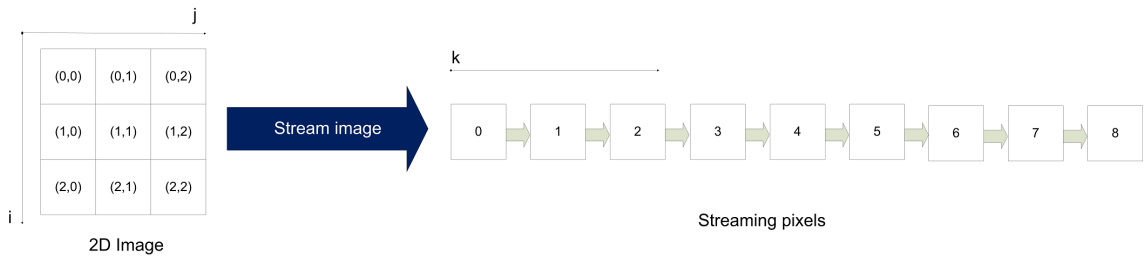


Figure 3.22: Stream an image into a pixel stream

The converting equations:

$$k = i * ImgHeight + j$$

$$i = k / ImgHeight$$

$$j = k \bmod ImgHeight$$

IP core submodules

The centroiding again is partitioned into submodules for specific purposes as shown in Figure 3.23.

- **stream processing:** The submodule task is to process the one-pass scan algorithm after receiving a pixel from the stream. The submodule also is in the responsibility of maintaining and updating the labels and disjoint sets data structures stored in the BRAM. The pseudo codes of the implementation are shown in Figure 3.24 and Figure 3.25

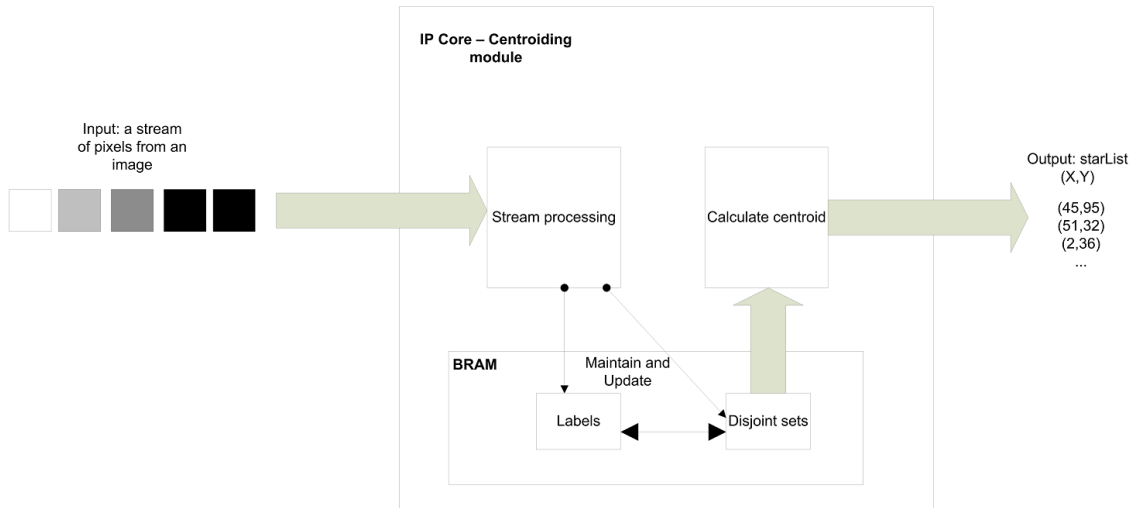


Figure 3.23: IP core submodules

- **centroid calculating:** The submodule task is to calculate the centroid coordinates after the stream processing stage is completed based on Equation 2.1. The inputs of the centroid calculating submodule is the disjoint sets data structures. The pseudo codes of the implementation are shown in Figure 3.26
- **BRAM:** served as the memory for the IP core. Stored the temporal data structures like: labels and disjoint sets and the final results(star centroid list).

```
def get_above_pixel(k):
    return k - imgHeight + (k mod imgHeight)

def get_left_pixel(k):
    return k + (k mod imgHeight) - 1
```

Figure 3.24: Get above and left pixel functions

3.3.2 Choose the reference star

Figure 3.28 shows a basic star image which will be processed through the Choose the reference star stage. The first Image in the example is a typical star image. The outer circle represents the FOV of the star Image, and the small blue dots represent the star clusters.


```

def stream_processing(current_pixel, disjoint_sets, labels):
    # get all pixel postions
    above_pixel = get_above_pixel(current_pixel)
    left_pixel = get_left_pixel(current_pixel)

    # Apply the one-pass scan algorithm
    ## Case 1: Both are background pixels
    if (above_pixel == BACKGROUND) and (left_pixel == BACKGROUND):
        cur_label = labels.create_new_label()
        current_pixel.set_label(cur_label)
        disjoint_sets.create(cur_label)

    ## Case 2: One(either pixel) is labeled, the other is not or
    ##           both are labeled with the same number
    else if isLabeled(above_pixel) or isLabeled(left_pixel) or
            get_label(above_pixel) == get_label(left_pixel):
        cur_label = labels.get_label(above_pixel)
        current_pixel.set_label(cur_label)

    ## Case 3: Both are labeled with different numbers
    else if get_label(above_pixel) != get_label(left_pixel):
        above_pixel_label = labels.get_label(above_pixel)
        left_pixel_label = labels.get_label(left_pixel)
        cur_label = above_pixel_label
        current_pixel.set_label(cur_label)
        disjoint_sets.join(above_pixel_label, left_pixel_label)

```

Figure 3.25: Stream processing submodule

```

def calculate_centroid():
    centroidList = list()
    for each set in disjoint_sets:
        total_intensity = 0
        (x,y) = (0,0)
        for each pixel in set:
            x += pixel.x() * pixel.Intensity()
            y += pixel.y() * pixel.Intensity()
            total_intensity += pixel.Intensity()
        X = x / total_intensity
        Y = y / total_intensity
        centroidList.add(X,Y)

    return centroidList

```

Figure 3.26: centroid calculating submodule

```
def centroiding():
    # Initiate
    disjoint_sets.Initiate()
    labels.Initiate()

    # submodule: Process stream
    while(receiving_input_pixel() and not timeout()):
        current_pixel = receiving_input_pixel()
        stream_processing(current_pixel, disjoint_sets, labels)

    # submodule: calculate centroids
    centroidList = calculate_centroid(disjoint_sets)

    return centroidList
```

Figure 3.27: The complete IP core module

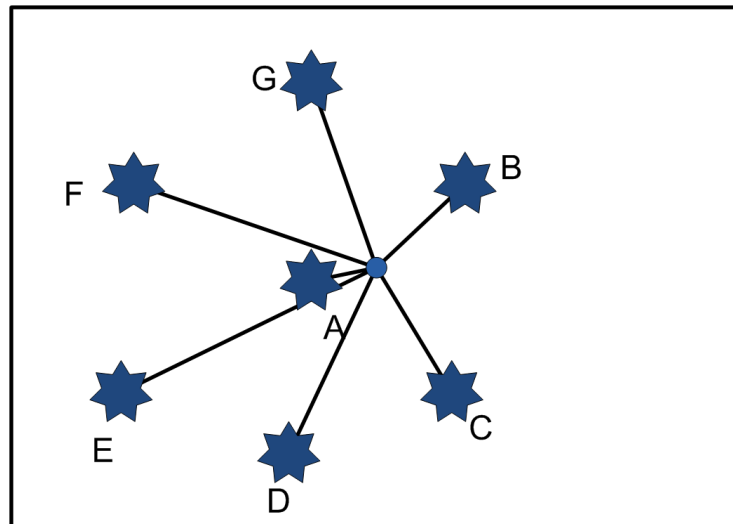


Figure 3.28: Distances from the centre of the image to all stars

We calculate the distances from each star cluster to the centre by Euclidean distance as given in equation 3.2. The star which is nearest to the centre (have the minimum distance value) will be chosen as the reference star.

$$d_{centre_to_star} = \sqrt{(x_{star} - x_{centre})^2 + (y_{star} - y_{centre})^2} \quad (3.2)$$

3.3.3 Find the star pattern

After we have the reference star, the next stage is to generate the star pattern. The number of stars in the image is counted, and their distances to the reference star are calculated using equation 3.3 to form a feature vector $f = \{N, D_1, D_2, D_3, D_n\}$

$$d_{centroid_to_star} = \sqrt{(x_{star} - x_{centroid})^2 + (y_{star} - y_{centroid})^2} \quad (3.3)$$

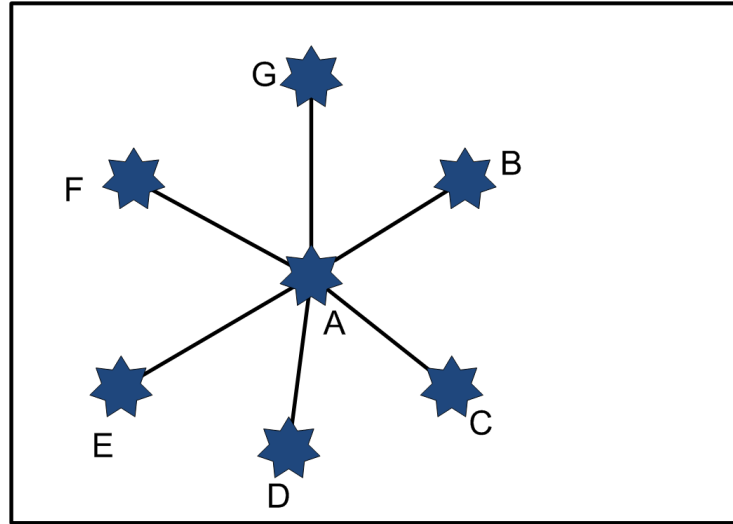


Figure 3.29: Distances from the reference star to its neighbors

3.3.4 Pattern searching

In the last stage, the feature vector is matched to the prebuilt tree pattern database. The feature vector from the Generate feature vector stage will be compared to the prebuilt tree structured star pattern database (SPD) to find the correct star cluster ID. Figure 3.30 shows how a star vector is compared and match with the SPD.

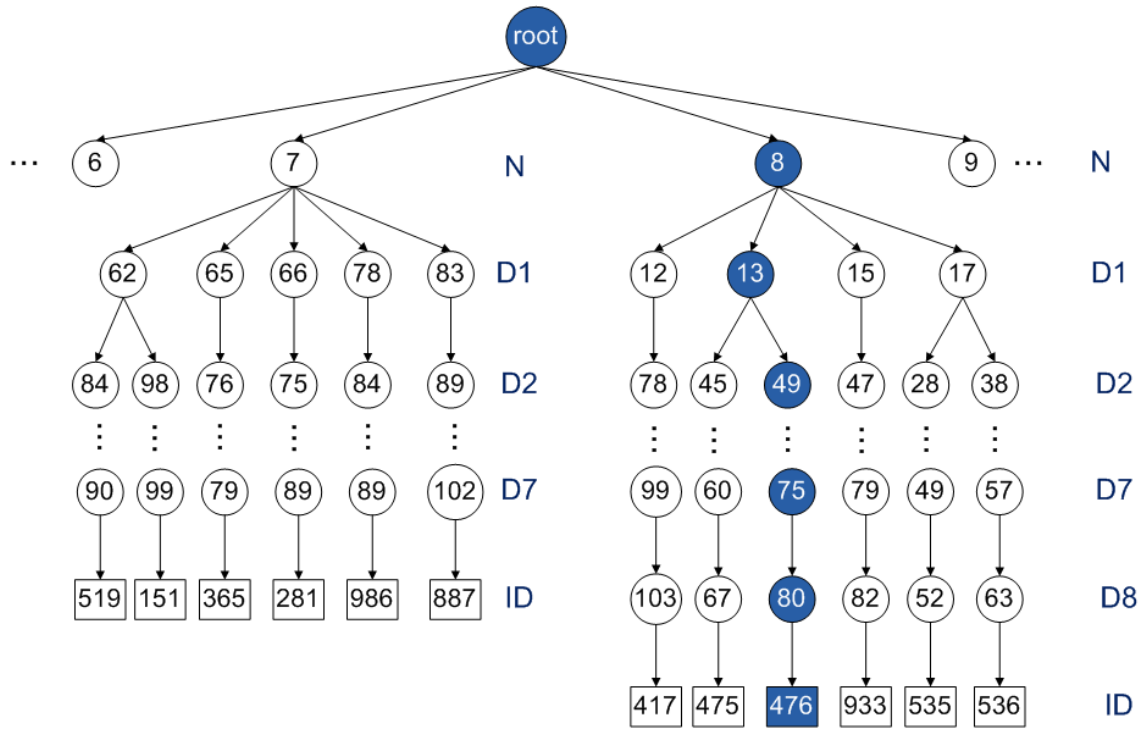


Figure 3.30: Star pattern matching

In case of mismatching, a tolerance will be added to research for another star ID. This search can be performed in parallel to increase the searching speed due to the specific tree structure of the prebuilt SPD as shown in Figure 3.31.

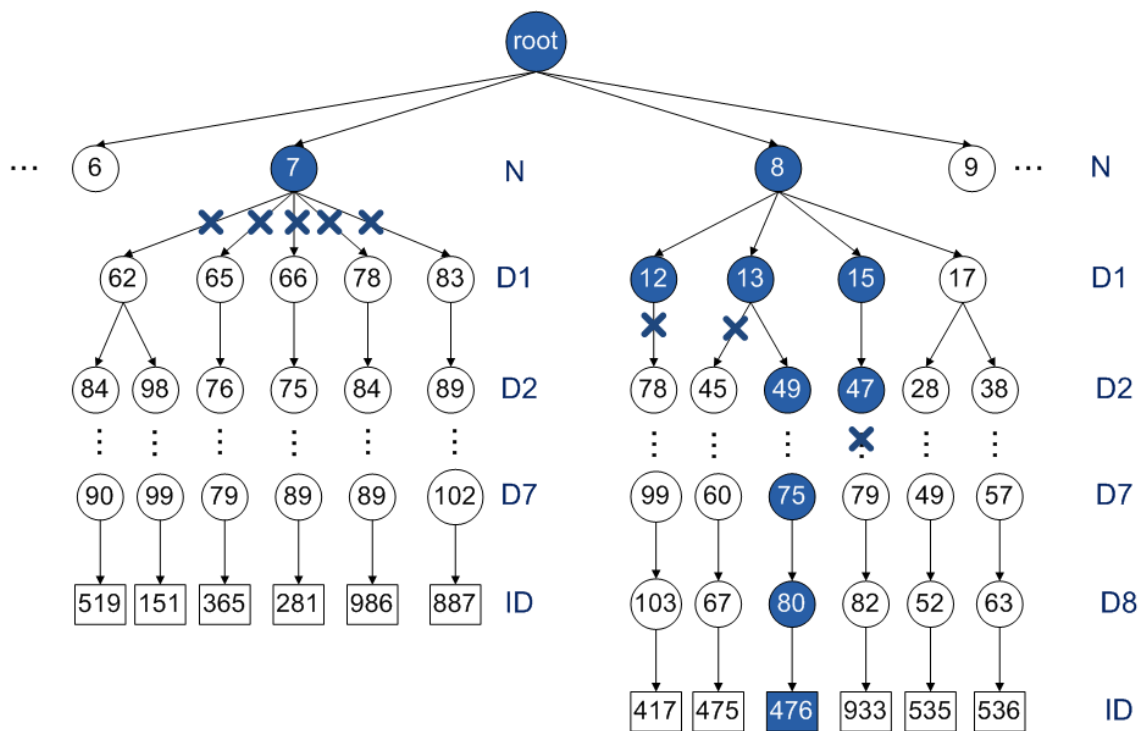


Figure 3.31: Star pattern matching with tolerance

Chapter 4

Experimental Results

4.1 Star data analysis

The main factors affect the runtime of the designed system are:

- Image resolution
- Number of stars in one image
- Star area (in pixels) of one star

If the resolution of the star image is large, the runtime and complexity of the algorithm will increase. Therefore, more optimizations are needed in both the hardware and the software of the system. Number of stars in one image is another aspect that we should consider. Since we need to maintain a disjoint set data structure on hardware, we need to know the maximum and the average number of stars in one image. As shown in Figure 4.1, the maximum number of star in one image is 24. Therefore, we should pre-allocate around 50 disjoint sets. We also expect to see an average of 10-11 stars with an average of pixel area around 18-19 pixels over one star as in Figure 4.2. This information helps us to pre-allocate the hardware memory BRAM and optimize it if needed.

The images simulated are based on the SSAO star catalog and the standard ESO star map. Randomized distribution of false stars are added to each image. For each resolution dataset, we have 12530 simulated images.

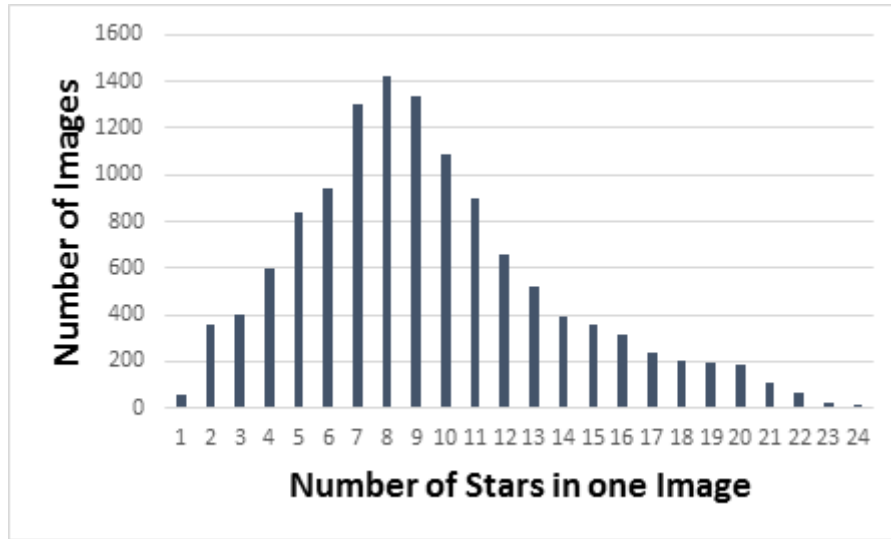


Figure 4.1: Number of stars in one image distribution

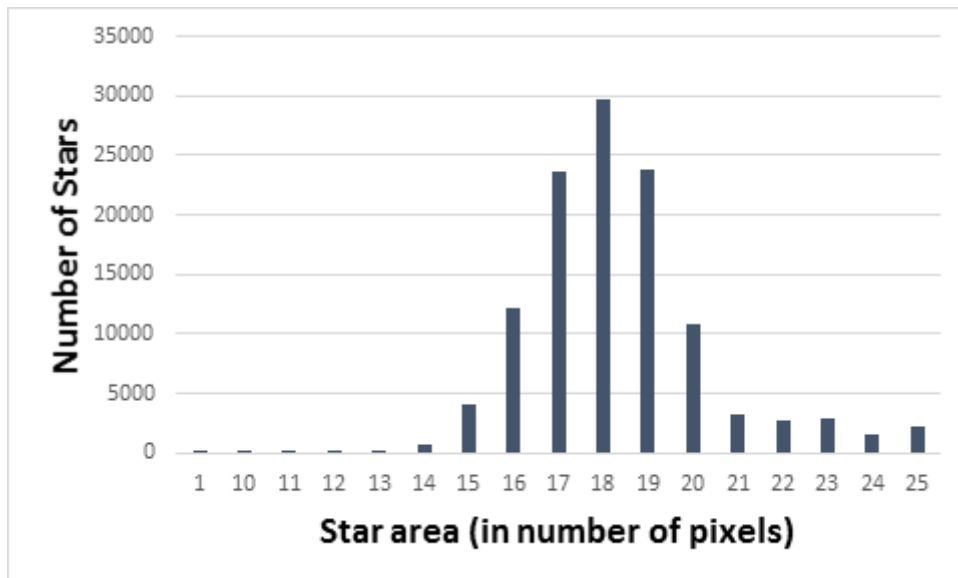


Figure 4.2: Star area distribution

The algorithm runtime performance is then compared between the implementation run on the embedded processor and the application executed on software-hardware co-processing strategy.

4.2 Hardware design

4.2.1 Components and Design Flow

The system design are shown in Figure 4.3. The IP modules as represented by Xilinx Vivado software are illustrated in Figure 4.4. The system includes several components such as:

- Processing system.
- Centroiding IP core.
- Direct Memory Access controlling system.
- BRAM
- Hardware timer
- Interrupt controller

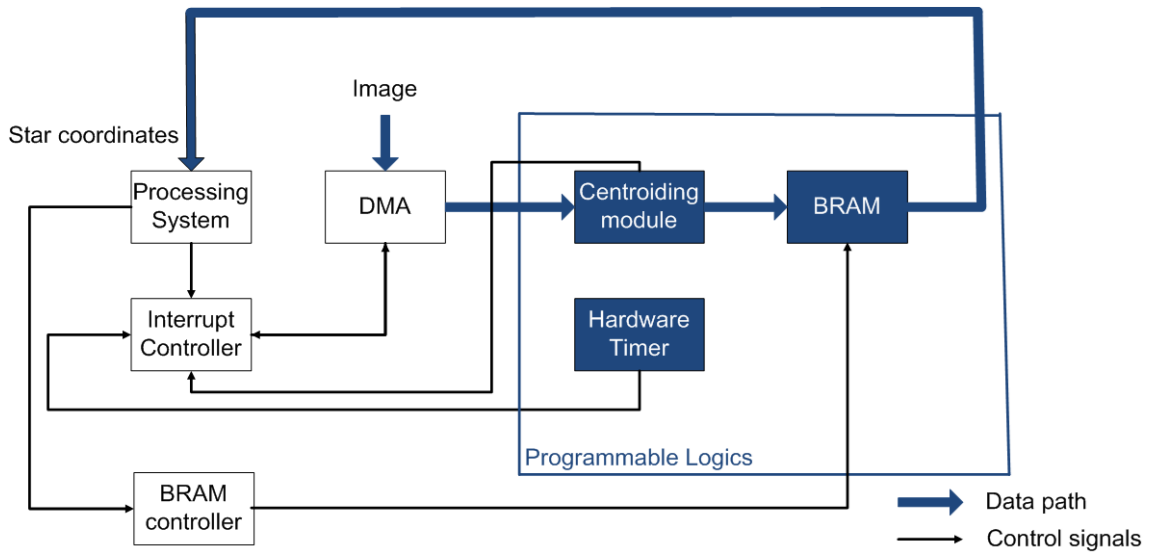


Figure 4.3: Hardware design diagram

Data path

The pixel data are streamed directly into memory by DMA module. The IP core is designed for processing the centroiding algorithm as soon as the first pixel data arrived. After finishing the centroiding algorithm, the IP core stores the results of centroiding algorithm into BRAM and informs the PS by an interrupt signal. PS then takes the results from BRAM and processes the other stages. The data path is implemented through AXI.

Control signals

The PS and PL side communicate through an interrupt controller. The interrupt controller informs the PS if the centroiding algorithm or hardware timer has finished, informs the DMA controller if the memory is full. The DMA controller then flushes the old data to free the memory. BRAM controller is a dual channel BRAM which is readable from PS side and writable from PL side.

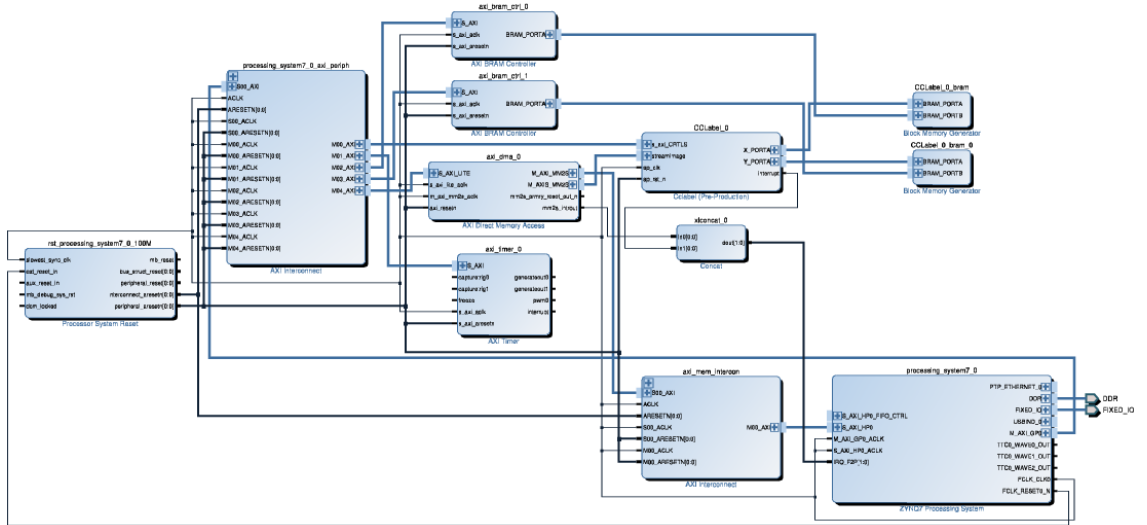


Figure 4.4: Hardware design block

Table 4.1 shows the percentage of hardware resources used over the available resources from the zedboard. We still have spare resources of the FPGA for other tasks.

Table 4.1: Hardware resource consumption

| Resource | Used | Available | Percentage (%) |
|---------------|-------|-----------|----------------|
| BRAM_18K | 17 | 280 | 6.07 |
| DSP48E | 20 | 220 | 9.09 |
| FlipFlops | 9278 | 106400 | 8.72 |
| Lookup Tables | 13387 | 53200 | 25.16 |

4.2.2 Power Analysis

The power consumption of the design is measured based on the condition described in Table 4.2.

Table 4.2: Environment condition

| Condition | value |
|---------------------|---------|
| Ambient temperature | 30.0°C |
| Airflow | 250 LFM |
| heat sink | medium |
| board temperature | 25.0°C |

As in Figure 4.5 and Figure 4.6, the Processing System(the ARM A9 processor) consumes 77% of the power supplied while other hardware components like the IP core, BRAM consume less power. This is due to the fact that generic processors are designed for multiple purpose tasks; hence they are not optimal for power consumption compared to the hardware solution for a specific task.

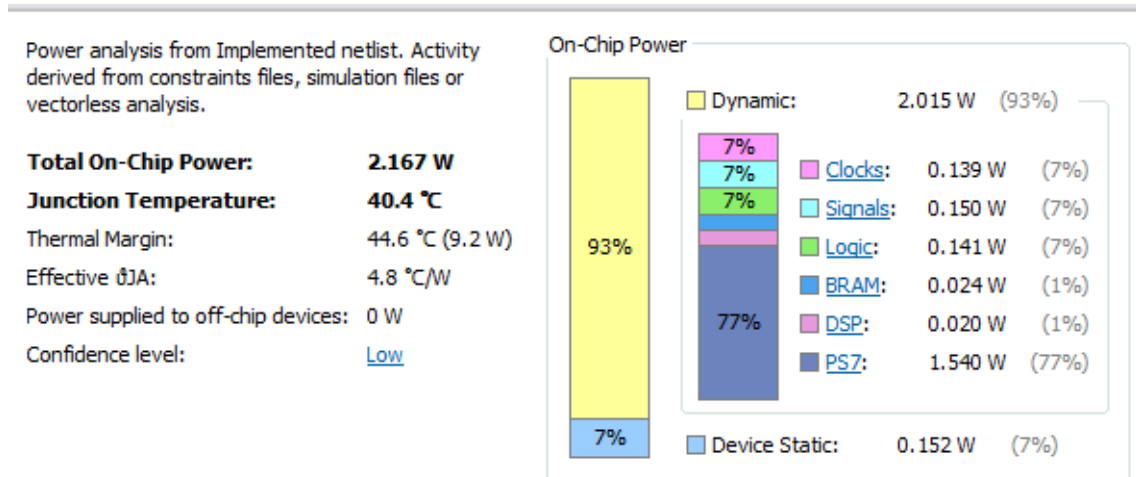


Figure 4.5: Power consumption summary

| Utilization | Name | Clocks (W) | Signals (W) | Data (W) | Clock Enable (W) | Set/Reset (W) | Logic (W) | BRAM (W) | DSP (W) | PS7 (W) | Processor (W) |
|--------------------------|-------------------------------------|------------|-------------|----------|------------------|---------------|-----------|----------|---------|---------|---------------|
| 2.015 W (93% of total) | design_1_wrapper | | | | | | | | | | |
| 2.015 W (93% of total) | design_1_1 (design_1_1) | 0.139 | 0.15 | 0.145 | 0.004 | 0.001 | 0.141 | 0.024 | 0.02 | 1.54 | 0.277 |
| 1.544 W (71% of total) | processing_system7_0 (design_1_1_0) | <0.0001 | 0.004 | 0.004 | <0.0001 | <0.0001 | <0.0001 | <0.0001 | <0.0001 | 1.54 | 0.277 |
| 1.544 W (71% of total) | inst (processing_system7_v5_5_p... | <0.0001 | 0.004 | 0.004 | <0.0001 | <0.0001 | <0.0001 | <0.0001 | <0.0001 | 1.54 | 0.277 |
| 0.353 W (16% of total) | CCLabel_0 (design_1_CCLabel_0_0) | 0.09 | 0.117 | 0.115 | 0.001 | <0.0001 | 0.115 | 0.01 | 0.02 | <0.0001 | <0.0001 |
| 0.352 W (16% of total) | inst (CCLabel) | 0.09 | 0.117 | 0.115 | 0.001 | <0.0001 | 0.115 | 0.01 | 0.02 | <0.0001 | <0.0001 |
| <0.0001 W (<1% of total) | Leaf Cells (41) | | | | | | | | | | |
| 0.064 W (3% of total) | processing_system7_0_axi_peri... | 0.028 | 0.019 | 0.018 | 0.002 | <0.0001 | 0.016 | <0.0001 | <0.0001 | <0.0001 | <0.0001 |
| 0.018 W (1% of total) | axi_dma_0 (design_1_axi_dma_0_0) | 0.009 | 0.002 | 0.001 | <0.0001 | <0.0001 | 0.002 | 0.006 | <0.0001 | <0.0001 | <0.0001 |
| 0.007 W (1% of total) | axi_timer_0 (design_1_axi_timer_... | 0.002 | 0.002 | 0.002 | <0.0001 | <0.0001 | 0.003 | <0.0001 | <0.0001 | <0.0001 | <0.0001 |
| 0.007 W (1% of total) | axi_mem_intercon (design_1_axi_... | 0.004 | 0.002 | 0.001 | <0.0001 | <0.0001 | 0.001 | <0.0001 | <0.0001 | <0.0001 | <0.0001 |
| 0.007 W (1% of total) | axi_bram_ctrl_0 (design_1_axi_br... | 0.003 | 0.002 | 0.002 | <0.0001 | <0.0001 | 0.002 | <0.0001 | <0.0001 | <0.0001 | <0.0001 |
| 0.007 W (1% of total) | axi_bram_ctrl_1 (design_1_axi_br... | 0.003 | 0.002 | 0.002 | <0.0001 | <0.0001 | 0.002 | <0.0001 | <0.0001 | <0.0001 | <0.0001 |
| 0.004 W (<1% of total) | CCLabel_0_bram (design_1_CCLa... | <0.0001 | <0.0001 | <0.0001 | <0.0001 | <0.0001 | <0.0001 | 0.004 | <0.0001 | <0.0001 | <0.0001 |
| 0.004 W (<1% of total) | CCLabel_0_bram_0 (design_1_CCLa... | <0.0001 | <0.0001 | <0.0001 | <0.0001 | <0.0001 | <0.0001 | 0.004 | <0.0001 | <0.0001 | <0.0001 |
| <0.0001 W (<1% of total) | rst_processing_system7_0_100N... | <0.0001 | <0.0001 | <0.0001 | <0.0001 | <0.0001 | <0.0001 | <0.0001 | <0.0001 | <0.0001 | <0.0001 |

Figure 4.6: Power consumption by components

4.3 Runtime experiments

4.3.1 512x512 dataset

The first dataset is generated by a MATLAB sky simulator software. It simulates the star images captured by the star tracker at specific attitudes. A simulated star tracker is configured as Table 4.3. It has 20° field of view (FOV) and can capture the stars that have magnitude threshold M_v less than 5.0. The star camera's attitude is rotated from 0 to 360° right ascension and from -90° to 90° declinations with an angle increment of 2° to perform a full scan of all the stars from the SAO SKY 2000 star catalogue. The dataset has total 12530 sky images.

Table 4.3: Star tracker configuration

| Parameters | Value |
|----------------------------|-----------------------|
| Field of View (FOV) | $20^\circ * 20^\circ$ |
| Visual magnitude threshold | 5.0 |
| Star catalogue | SAO SKY 2000 |
| Number of samples | 12530 |

A. Software runtime

The algorithm is developed on the zedboard processing system which runs on an 1.0 GHz ARM-A9 CPU with 512 MB DDR3 RAM. The algorithm software performance is described in Table 4.4 and visualized by Figure 4.7. The runtime of 4 modules are measured in both average and worst-case over 12530 sky images.

As we know from the profiling stage, the runtime of the centroiding module is the most critical time-consuming part. It can be explained that this stage deals with image processing which is the highest complexity in computation compared to the 3 remaining stages.

Thus, the worstcase runtimes are not far from the averages. This pattern can be explained by the number of stars in one Image and the star area distribution. The distributions are approximately uniform with low standard deviations. Therefore,

our system can run stably despite different configuration.

Overall, The average runtime is 17855 us (about 17.86 ms) on each image.

Table 4.4: Software runtime

| | Average | Worst case |
|--------------------------------|---------|------------|
| Centroiding | 17688 | 18061 |
| Choosing Reference Star | 54 | 105 |
| Finding Star Pattern | 30 | 109 |
| Pattern Matching | 83 | 155 |

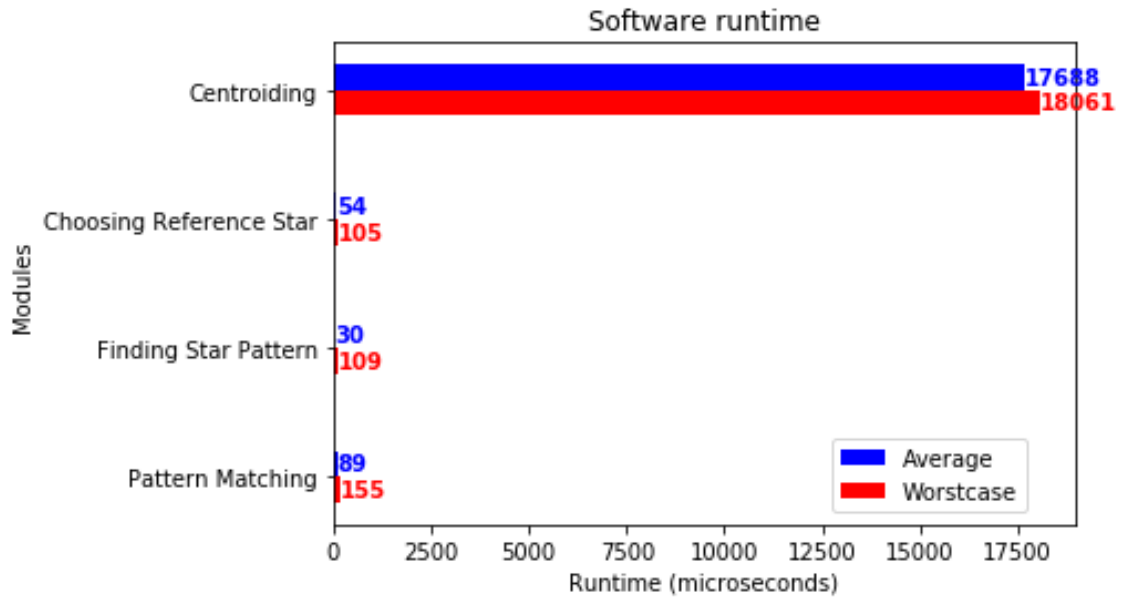


Figure 4.7: Software runtime

B. Hardware - Software co-processing runtime

The algorithm is re-developed on the zedboard in both the processing system(software) and the programmable logic(hardware). The processing system runs on an 1.0 GHz ARM-A9 CPU with 512 MB DDR3 RAM while the programmable logic runs on the FPGA fabric with 100 MHz Clock rate and a total of 560KB BRAM (Block RAM). The algorithm is partitioned into 6 submodules. The first 3 submodules: IP core Initiation, DMA Data Streaming and Centroiding are implemented on the programmable logic side. The 3 remaining submodules: Choosing Reference Star, Finding Star Pattern and Pattern Matching are implemented on the processing system. The system performance is described in Table 4.5 and visualized by Figure 4.8.

The Centroiding software submodule is replaced by 3 equivalent hardware submodules. The runtime is significantly improved from nearly 17 ms to nearly 6.2 ms.

The average total runtime is 6352 us(about 6.35 ms).

Table 4.5: Hardware Software Co-processing runtime

| | Average | Worst case |
|--------------------------------|----------------|-------------------|
| IP core Initiation | 6 | 6 |
| DMA Data Streaming | 2460 | 2485 |
| Centroiding | 3719 | 3806 |
| Choosing Reference Star | 54 | 145 |
| Finding Star Pattern | 30 | 109 |
| Pattern Matching | 83 | 155 |

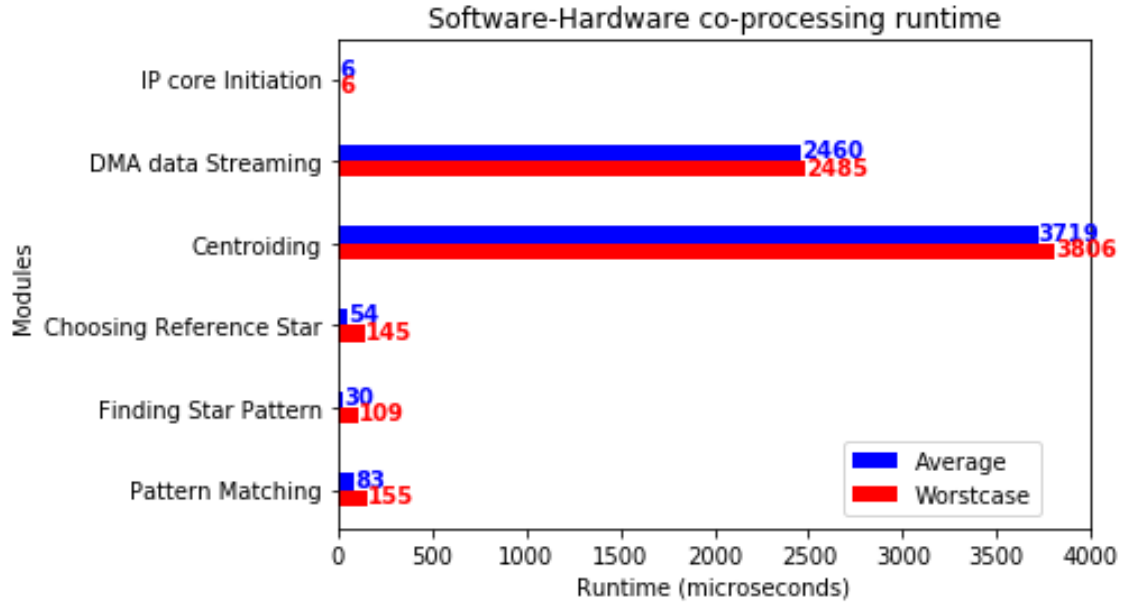


Figure 4.8: Software - Hardware co-processing runtime

4.3.2 1024x1024 dataset

Next, we perform a study on 1019 star images are captured by the star tracker SST-20S currently mounted on a low earth orbit satellite, VELOX-CI[1]. The specifications of the SST-20S star tracker is described by Table 4.9.

Table 4.6: Specifications of the SST-20S star tracker and the real image[1]

| Parameter | Value |
|-----------------------|---------------------------|
| Field of View (FOV) | $15^{\circ} * 15^{\circ}$ |
| Sensitivity (Mv) | 6.3 |
| Star catalog | SAO J2000[32] |
| Resolution (w * h) | 1024 x 1024 pixels |
| Pixel size (ρ) | 13 m |
| Focal length (f) | 50 mm |
| Bits per pixel | 8 |
| Position accuracy | 40 arcsec |

A. Software runtime

The algorithm is examined again on the zedboard processing system (1.0 GHz ARM-

A9 CPU, 512 MB DDR3 RAM). Its performance is listed in Table 4.7 and visualized by Figure 4.9. The runtime of 4 modules is measured in both average and worst-case over 1019 sky images.

As the image size increased, the runtime of the Centroiding part increases and other module runtimes remain approximately the same. We can explain that the runtime of the centroiding part is proportional to the complexity of the image processing task, while other module complexities depend on the properties of the images which are the number of stars, the brightness of the star catalog threshold.

The average runtime is 70780 us (about 70.78 ms). The runtime has increased 4 times (70 ms compared to 17 ms).

Table 4.7: Software runtime

| | Average | Worst case |
|--------------------------------|----------------|-------------------|
| Centroiding | 70527 | 70561 |
| Choosing Reference Star | 63 | 108 |
| Finding Star Pattern | 54 | 115 |
| Pattern Matching | 136 | 155 |

B. Hardware - Software Co-processing runtime

We again tested the algorithm on the large dataset with the Zedboard System-on-a-chip Processing System and Programmable Logic (PS - PL). The system performance is described in Table 4.8 and visualized by Figure 4.10.

The total runtime of the Centroiding module is around 13.3 ms. Compared to 6.35 ms of the small dataset runtime (512x512), the Hardware-Software Centroiding submodule runtime only increases 2 times. As we look further into each submodule, the DMA Data Streaming submodule runtime has a significant change (2.4 ms to 9.8 ms) while the Centroiding submodule runtime is stable (3.7 ms and 3.5 ms). This can be explained by the hardware design has been proposed and introduced in Chapter 4.2 “Hardware design”. The DMA Data Streaming submodule streams

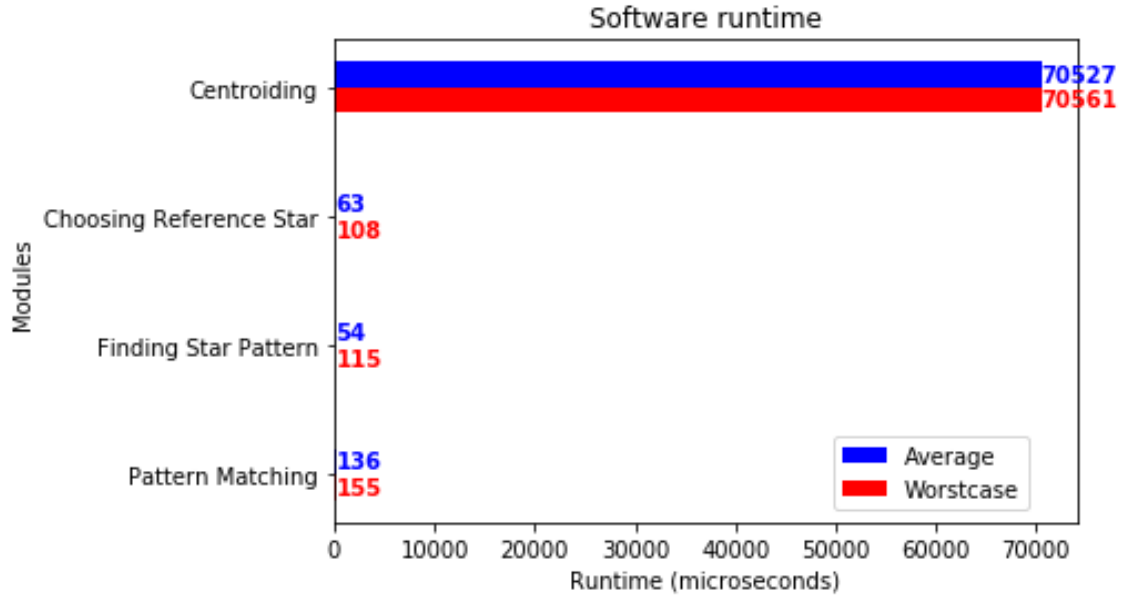


Figure 4.9: Software runtime

the image pixels into the system memory, it is the only submodule that affected by the image size complexity. Because the Hardware-Software Centroiding submodule takes the pixel coordinates as inputs, this architecture design helps our system run stably despite the changing of the image size.

The total average runtime is 13636 us (about 13.64 ms).

Table 4.8: Hardware - Software Co-processing runtime

| | Average | Worst case |
|--------------------------------|---------|------------|
| IP core Initiation | 6 | 6 |
| DMA Data Streaming | 9834 | 9838 |
| Centroiding | 3543 | 3598 |
| Choosing Reference Star | 63 | 108 |
| Finding Star Pattern | 54 | 115 |
| Pattern Matching | 136 | 155 |

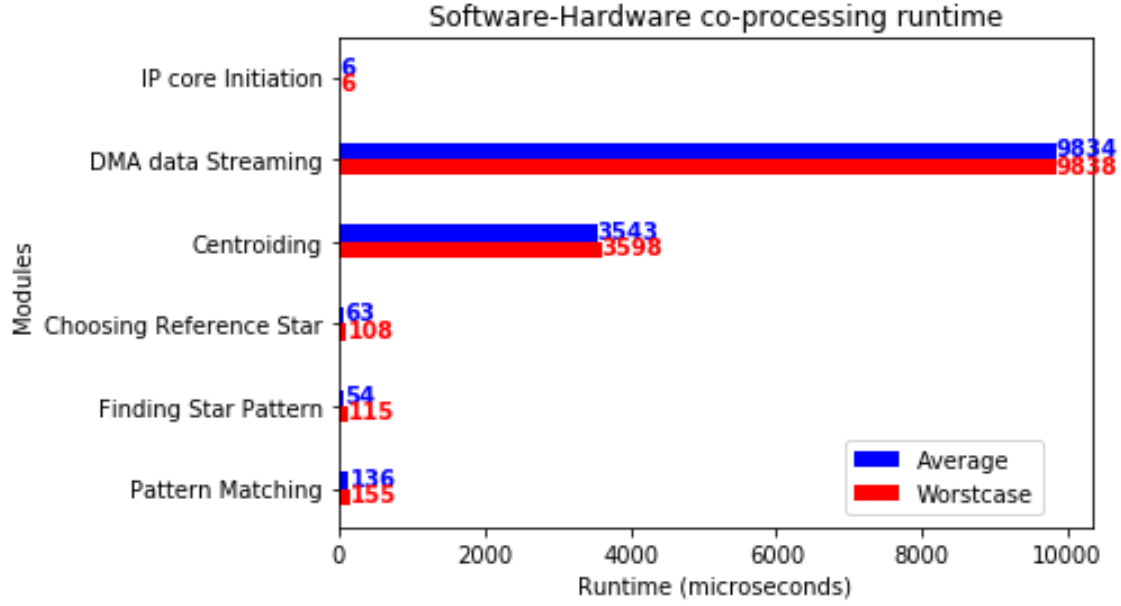


Figure 4.10: Hardware - Software Co-processing runtime

4.3.3 Runtime Comparison

Lastly, we perform the final test to compare the runtimes of the 3 classic algorithms and the proposed algorithm by software processing against the proposed algorithm by software-hardware co-processing. The experiment results are benchmarked in Table 4.9 and visualized by Figure 4.11.

The software system is implemented on the zedboard with a 1.0 GHz ARM-A9 CPU and 512 MB DDR3 RAM. The hardware-software co-processing system is executed on the zedboard Processing system -Programmable Logic with a 1.0 GHz ARM-A9 CPU, 512 MB DDR3 RAM (PS) and the FPGA fabric with 100 MHz Clock rate, 560KB BRAM (PL).

The experimental results show that the implementation of the proposed method by software-hardware co-processing has successfully reduced the runtime of the Lost-in-Space star tracking algorithm.

Table 4.9: Runtime comparison

| | Average(ms) | Worst case(ms) |
|------------------------------------|-------------|----------------|
| Liebe method SW | 190.6 | 304.7 |
| Geometric voting method SW | 958.4 | 1044.7 |
| Pyramid method SW | 352.3 | 576.6 |
| Proposed method SW | 70.8 | 70.9 |
| Proposed method SW-HW coprocessing | 13.6 | 13.8 |

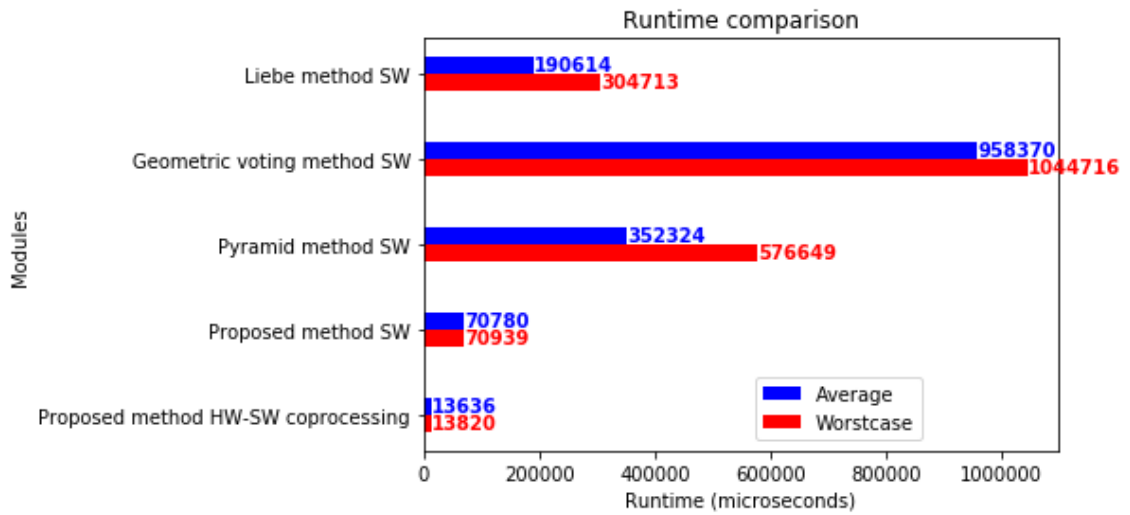


Figure 4.11: Runtime comparison

Chapter 5

Summary and Future Works

5.1 Summary

The purpose of this research topic is to implement a system evaluating a star tracking algorithm proposed by Mr. Minh Duc Pham[8, 12, 13], my senior and an ex post-graduated NTU student. In my thesis, I have summarized three traditional methods and one state-of-the-art star tracking method proposed in the literature review section. Then in the Hardware and Software Co-processing Implementation of the Algorithm section, I introduced the hardware system, deeply analyze the algorithm. I also proposed an adaptive algorithm based on the proposed algorithm that is suitable for the software-hardware co-processing implementation in the system. In the final section Experimental Results, I suggested my hardware architecture design for this project, carry out some experiments to evaluate the implementation and their results.

All of my work includes the simulation image generator, image datasets, hardware IP core design, system architecture, software algorithms and source code, results of the experiments, quick documentations are dedicated in this repository: <https://github.com/dangkhoatl/Master-Thesis-Star-Tracking-System>

5.2 Future Works

Currently, the system can not handle a high throughput image data streaming. In my experiments, I have to handle the images one-by-one to feed into the system.

Hence, I suggest implementing an input-processing module with can manage a large stream amount of image data(around 9.8 GBs) autonomously.

Moreover, the first dataset is generated by sky simulation with slightly normal distribution noise added, the second dataset is captured by a star tracker from the ground. In space, there are more noises affect the quality of the images from the electromagnetic field, Solar noise, Cosmic noise, etc. A noise cancellation module implemented in the PL would be needed.

Bibliography

- [1] M D Samirbhai, S Chen, and K S Low. A hamming distance and spearman-correlation based star identification algorithm. *IEEE Transactions on Aerospace and Electronic Systems*, page 1, 2018.
- [2] Scherr Timothy. Introduction to FPGA Design for Embedded Systems.
- [3] Xilinx.com. *Spartan-3AN FPGA Family datasheet*. 2014.
- [4] Louise Crockett, Ross Elliot, Martin Enderwitz, Bob Stewart, and David Northcote. *The Zynq Book: Embedded Processing with the Arm Cortex-A9 on the Xilinx Zynq-7000 All Programmable Soc*. Strathclyde Academic Media, 2015.
- [5] BBC Worldwide Ltd., Films for the Humanities Sciences Firm, and Films Media Group. In Orbit How Satellites Rule Our World, 2013.
- [6] Wikipedia. Satellite.
- [7] Walter Colitti, Kris Steenhaut, Nicolas Descouvemont, and Adam Dunkels. Satellite based wireless sensor networks: global scale sensing with nano- and pico-satellites., 2008.
- [8] Minh Duc Pham. *Attitude determination system for nano-satelite*. PhD thesis, Nanyang Technological University, 2013.
- [9] M D Shuster and S D Oh. Three-axis attitude determination from vector observations. *Journal of Guidance, Control, and Dynamics*, 4(1):70–77, 1981.
- [10] Star trackers for attitude determination. *IEEE Aerospace and Electronic Systems Magazine, Aerospace and Electronic Systems Magazine, IEEE, IEEE Aerosp. Electron. Syst. Mag*, (6):10, 1995.

- [11] James Richard Wertz. *Spacecraft attitude determination and control*. Astrophysics and space science library: v. 73. Dordrecht ; London : Kluwer Academic Publishers, c1978., 1978.
- [12] M D Pham, K S Low, Shoushun Chen, and Y T Xing. A star pattern recognition algorithm for satellite attitude determination. In *ISIEA 2012 - 2012 IEEE Symposium on Industrial Electronics and Applications*, number ISIEA 2012 - 2012 IEEE Symposium on Industrial Electronics and Applications, pages 236–241, School of Electrical and Electronic Engineering, Nanyang Technological University, 2012.
- [13] An Autonomous Star Recognition Algorithm with Optimized Database. *IEEE Transactions on Aerospace and Electronic Systems, Aerospace and Electronic Systems, IEEE Transactions on, IEEE Trans. Aerosp. Electron. Syst.*, (3):1467, 2013.
- [14] Steve B Howell. *Handbook of CCD astronomy*. Cambridge observing handbooks for research astronomers: 5. Cambridge ; New York : Cambridge University Press, 2006., 2006.
- [15] Pattern recognition of star constellations for spacecraft applications. *IEEE Aerospace and Electronic Systems Magazine, Aerospace and Electronic Systems Magazine, IEEE, IEEE Aerosp. Electron. Syst. Mag.*, (1):31, 1993.
- [16] Accuracy performance of star trackers - A tutorial. *IEEE TRANSACTIONS ON AEROSPACE AND ELECTRONIC SYSTEMS*, 38(2):587–599.
- [17] Micro APS based star tracker. *Proceedings, IEEE Aerospace Conference, Aerospace Conference Proceedings, 2002. IEEE, Aerospace conference*, page 5, 2002.
- [18] Star tracker design considerations for the Europa Orbiter mission. *1999 IEEE Aerospace Conference. Proceedings (Cat. No.99TH8403), Aerospace Conference, 1999. Proceedings. 1999 IEEE*, page 67, 1999.
- [19] Ying Dong, Fei Xing, and Zheng You. Brightness Independent 4-Star Matching Algorithm for Lost-in-Space 3-Axis Attitude Acquisition. *Tsinghua Science & Technology*, 11:543–548, 2006.

- [20] D Mortari, John Junkins, and Malak Samaan. Lost-in-Space Pyramid Algorithm for Robust Star Pattern Recognition. 2001.
- [21] D Mortari and Beny Neta. k-Vector Range Searching Technique. 105, 2000.
- [22] D Mortari, Malak Samaan, Christian Bruccoleri, and John Junkins. The Pyramid Star Identification Technique. *NAVIGATION*, 51, 2004.
- [23] Benjamin B. Spratling and D Mortari. A Survey on Star Identification Algorithms. *Algorithms*, 2, 2009.
- [24] Crew, Vanderspek G. B., R., and Doty J. HETE Experience with the Pyramid Algorithm. *MIT Center for Space Research, Cambridge, MA, 02139 USA*, 2002.
- [25] Geometric voting algorithm for star trackers. *IEEE Transactions on Aerospace and Electronic Systems, Aerospace and Electronic Systems, IEEE Transactions on, IEEE Trans. Aerosp. Electron. Syst.*, (2), 2008.
- [26] Andrew Moore. *FPGAs for Dummies*. 2014.
- [27] Wikipedia. Semiconductor intellectual property core.
- [28] Jens Rettkowski, Andrew Boutros, and Diana Göhringer. HW/SW Co-Design of the HOG algorithm on a Xilinx Zynq SoC. *Journal of Parallel & Distributed Computing*, 109:50–62, 2017.
- [29] Tony Grant. *Xilinx Redefines Power, Performance, and Design Productivity with Three Innovative 28 nm FPGA Families: Virtex-7, Kintex-7, and Artix-7 Devices*. 2011.
- [30] Donald Bailey, Christopher Johnston, and Ni Ma. Connected components analysis of streamed images, 2008.
- [31] Michael J Klaiber, Yousef O Baroud, Sven Simon, and Donald G Bailey. A Resource-Efficient Hardware Architecture for Connected Component Analysis. *IEEE TRANSACTIONS ON CIRCUITS AND SYSTEMS FOR VIDEO TECHNOLOGY*, 26(7):1334–1349.

- [32] J R Myers, C B Sande, A C Miller, W H Warren Jr, and D A Tracewell.
SKY2000-master star catalog-star catalog database. *Bulletin of the American
Astronomical Society*, 191(128.12), 1997.